Excited State Structural Events of a Dual-Emission Fluorescent Protein Biosensor for Ca 2+ Imaging Studied by Femtosecond Stimulated Raman Spectroscopy

ARTICLE *in* THE JOURNAL OF PHYSICAL CHEMISTRY B · SEPTEMBER 2014

Impact Factor: 3.3 · DOI: 10.1021/jp505698z · Source: PubMed

Excited State Structural Events of a Dual-Emission Fluorescent Protein Biosensor for Ca^{2+} Imaging Studied by Femtosecond Stimulated Raman Spectroscopy

Yanli Wang,[a] Longteng Tang,[a] Weimin Liu,[a] Yongxin Zhao,[b] Breland G. Oscar,[a] Robert E. Campbell,[b] and Chong Fang[a,1]

[a]Department of Chemistry, Oregon State University, Corvallis, OR 97331-4003, U.S.A.; and

[b]Department of Chemistry, University of Alberta, Edmonton, Alberta T6G 2G2, Canada

[1]To whom correspondence should be addressed. E-mail: Chong.Fang@oregonstate.edu.

Phone: 541-737-6704.

RECEIVED DATE (to be automatically inserted after your manuscript is accepted if required according to the journal that you are submitting your paper to *JPCB*)

Abstract (≤200 words)

Fluorescent proteins (FPs) are luminescent biomolecules that emit characteristic hues upon irradiation. A group of calmodulin (CaM)-green FP (GFP) chimeras have been previously engineered to enable the optical detection of calcium ions (Ca^{2+}). We investigate one of these genetically encoded Ca^{2+} biosensors for optical imaging (GECOs), GEM-GECO1, which fluoresces green without Ca^{2+} but blue with Ca^{2+}, using femtosecond stimulated Raman spectroscopy (FSRS). The time-resolved FSRS data (<800 cm^{-1}) reveal that initial structural evolution following 400-nm photoexcitation involves small-scale coherent proton motions on both ends of the chromophore two-ring system with a <250 fs time constant. Upon Ca^{2+} binding, the chromophore adopts a more twisted conformation in the protein pocket with increased hydrophobicity, which inhibits excited-state proton transfer (ESPT) by effectively trapping the protonated chromophore in S_1. Both the chromophore photoacidity and local environment form the ultrafast structural dynamics basis for the dual-emission properties of GEM-GECO1. Its photochemical transformations along multidimensional reaction coordinates are evinced by distinct stages of FSRS spectral evolution, particularly related to the ~460 and 504 cm^{-1} modes. The direct observation of lower frequency modes provides crucial information about the nuclear motions preceding ESPT, which enriches our understanding of photochemistry and enables the rational design of new biosensors.

Keywords

Femtosecond stimulated Raman spectroscopy | Calcium-sensing fluorescent proteins | Fluorescence modulation mechanism | Excited state proton transfer | Ultrafast conformational dynamics

I. Introduction

The green fluorescent protein (GFP), first extracted and purified from a Pacific Northwest jellyfish *Aequorea victoria* in the 1960s,[1] is the archetype for the fluorescent protein (FP) superfamily. All of the members of this family, which include FPs with hues ranging from cyan through red, have been discovered in marine organisms, with reef corals being the most prolific source.[2,3] Since the genetic encodability of FPs was demonstrated as early as the 1990s, FPs have revolutionized molecular and cellular biology, enabling the visualization of life processes at a level of detail that would otherwise be experimentally inaccessible.[1-8] FPs are particularly useful for live cell imaging because they are genetically encodable, brightly fluorescent, and tolerant to a variety of structural manipulations (e.g., fusion, insertion, circular permutation, splitting). However, despite decades of extensive engineering, major limitations still exist for the current FPs (e.g., insufficient photostability, lack of bright near-infrared variants, slow folding rate, and blinking), which hinder their applications in some next-generation bioimaging applications[9-18] such as imaging beyond the optical diffraction limit[9-11,17] and single molecule detection.[19,20] So far, the majority of the protein engineering efforts have been concentrated on random mutagenesis, which typically requires a customized screening assay to optimize a specific function or attribute.[21,22] It is thus time-consuming and labor intensive, and cannot provide fundamental insights on the structure-function relationship of the protein system.[23,24]

The tolerance of FPs to structural manipulations has allowed protein engineers to convert FPs into FP-based biosensors that enable dynamic physiological processes to be visualized using fluorescence imaging. Many researchers and protein engineers are currently working to

expand the toolkit of FP-based biosensors in order to visualize cellular processes with better resolution, higher sensitivity, and faster kinetics, e.g., neural imaging[25,26] and physiological cellular sensing.[8,27,28] In particular, the ability to sense calcium ions (Ca^{2+}) in living systems has revolutionized the ability of researchers to image neuronal activity[25,26,29-31] and cancer metastasis,[32,33] among many other key biological processes. The most useful class of Ca^{2+} biosensors is the GCaMP family that is created from a fusion of GFP, calmodulin (CaM), and the M13 domain of a myosin light chain kinase.[34-37] These biosensors typically display an increase of fluorescence when Ca^{2+} is present and are hence useful for imaging cellular processes such as action potentials.[38]

We aim to improve the FP biosensors from a new structural dynamics perspective by understanding the fluorescence mechanism of FPs. This fundamental knowledge is crucial to rationally design FP biosensors at the molecular level. The three-residue autocyclized chromophore is the part of an FP that is responsible for its color, and is located near the center of the protein β-barrel.[39-41] Due to the π–π^* transition in the electronic domain, a typical UV/visible (UV/Vis) excitation source can induce characteristic fluorescence from all kinds of FP biosensors. Fluorescence lifetime is typically on the nanosecond (ns) timescale, but the molecular events leading to emission occur much faster, so we need to capture the structural evolution of the photoexcited chromophore on the femtosecond (fs) to picosecond (ps) timescale, ideally starting from time zero of electronic excitation. In essence, the suitable spectroscopic technique to achieve this goal to dissect the origin of fluorescence requires simultaneously high spatial (atomic-level) and temporal (fs) resolutions.[42-44]

The foundational knowledge of chromophore dynamics in FPs has been provided by

ultrafast spectroscopic techniques including time-resolved fluorescence,[39,45-47] transient absorption,[48,49] transient IR,[50-53] and IR pump-dump-probe measurements.[54] In particular, our earlier report on wild-type (wt)GFP uncovered a dominant 120 cm^{-1} phenol ring-wagging mode that gates the main photochemical event, excited state proton transfer (ESPT), following 400 nm photoexcitation.[42] Data analysis therein focused on the quantum beats observed for the high-frequency vibrational modes, i.e., >800 cm^{-1}. Notably, vibrational modes below 600 cm^{-1} are relatively difficult to study due to limited availability of IR pulses in that wavelength range (e.g., >17 μm) as well as small electric polarizability leading to weak Raman signal in general.[55] These lower frequency modes carry important information about collective skeletal motions of the chromophore that may have a strong projection onto the photochemical reaction coordinate.[42,56,57] Moreover, the direct observation of an array of vibrational modes in S_1 following photoexcitation affords a unique opportunity to investigate the non-equilibrium structural dynamics before the molecular system reaches its equilibrium polarization, particularly in correlation with transient atomic motions that are part of a highly exergonic reaction.

In this work, we track the transient structural evolution of the photoexcited chromophore inside a CaM-GFP chimera called GEM-GECO1,[28] which has been recently developed to detect nanomolar concentrations of Ca^{2+} under physiological conditions. GECO stands for genetically encoded Ca^{2+} biosensor for optical imaging. Compared to related Ca^{2+}-sensing proteins in the aforementioned GCaMP family,[25-27,29,30,35-37,58,59] GEM-GECO1 exhibits an intriguing dual-emission behavior as it emits green in the absence of Ca^{2+} but blue upon Ca^{2+} binding. We develop the femtosecond stimulated Raman spectroscopy (FSRS) protocol to

obtain a series of time-resolved excited-state vibrational spectra of the embedded chromophore following electronic excitation, and obtain new insights into the crucial *initial* stage of photoinduced structural evolution preceding ESPT. Aided by time-dependent density functional theory (TD-DFT) calculations,[60] we analyze the transient kinetic plots of three vibrational marker bands between 400 and 800 cm^{-1} in conjunction with high-frequency mode evolution.[61] Ultrafast frequency shifts in these lower frequency modes are analyzed to infer the initial phase of ESPT reaction in the context of Franck-Condon (FC) proton motions via pre-existing H-bonding chains. The data also shed light on the two-ring coplanarity of the chromophore in the electronic ground and excited states. This new level of mechanistic understanding lays the solid foundation for engineering FP biosensors from the bottom up.

II. Materials and Methods

The GEM-GECO1 proteins were purified from *E. coli* DH10B cells transformed with the pTorPE plasmid harboring 6-histidine tagged GEM-GECO1. Detailed sample preparation steps have been reported.[28,61] Briefly, a transformed *E. coli* colony harboring the aforementioned plasmid was picked and cultured in 1 L of a modified version of sterilized terrific broth (20 g LB mix, 14 g trytone, 7 g yeast extract, 9.2 g K_2HPO_4, 2.2 g KH_2PO_4, and 8 mL glycerol, pH=7.20) in a temperature-controlled shaker at 30 °C for 48 hours. The cells were collected by centrifugation and lysed by French press. After another round of centrifugation, GEM-GECO1 proteins in the soluble cell extract were purified by Ni-NTA affinity chromatography and buffer exchanged. Finally, concentrated GEM-GECO1 proteins (OD>10/cm at 400 nm) in MOPS buffer with either 10 mM EGTA (Ca^{2+}-free sample) or 10

mM CaEGTA (Ca^{2+}-bound sample) were used for *in vitro* spectroscopic characterization. The UV/Vis absorption spectra of the protein samples are shown in Figures 1 and S1.

Our experimental FSRS setup has been previously described.[62-64] In brief, a mode-locked Ti:Sapphire oscillator and a regenerative amplifier (Legend Elite-USP-1K-HE, Coherent, Inc.) provide ~4 W, 35 fs, 800 nm fundamental pulses with a 1 kHz repetition rate. Three pulses are generated from half of the laser output: (1) a narrowband Raman pump at ~800 nm, 3.5 ps, 6 mW from a home-built spectral filter, (2) a broadband Raman probe at ca. 820—910 nm, 40 fs, 100 μW from supercontinuum white light generation in a 2-mm-thick sapphire plate followed by prism compression, and (3) a broadband photoexcitation pulse at 400 nm, 40 fs, 500 μW from second-harmonic generation in Type-I BBO crystal and prism compression afterwards. All three *p*-polarized pulses are collimated and focused onto the sample solution, flowing through a 1-mm-pathlength cell chamber sandwiched by two 1-mm-thick fused quartz windows. The probe pulse carrying the stimulated Raman scattering signals is selected by a pinhole after the sample cell and sent through a spectrograph to be imaged onto a 1340×100 pixel-array front-illuminated CCD camera (PIXIS 100F, Princeton Instruments) that is synchronized with the fundamental laser repetition rate. Therefore, one FSRS spectrum can be obtained in 2 ms from the ratio of the Raman probe spectra with Raman pump "on" over "off" that is controlled by a 500 Hz optical chopper in the pump beampath.[62,63]

The protein is prepared at OD ≈ 1/mm at the main absorption peak (~400 nm) to achieve a relatively transparent sample solution with enough Raman peak intensity.[42] The spectra are collected following ~500 μW, 400 nm photoexcitation pulse with an 800 nm Raman pump, across a spectral window spanning from ca. 350—1450 cm^{-1}. To monitor the sample

condition and long-term stability of the fs laser system, the ground-state (S_0) Raman spectrum is periodically collected throughout the excited-state (S_1) data collection period. The S_0 spectrum is then averaged and fitted by multiple gaussian peaks (Supporting Information). A small percentage of the fitted S_0 spectrum, ~10% in this work for both Ca^{2+}-free and bound proteins, is added back to the ground-state-subtracted excited-state FSRS spectra, in order to obtain the pure excited-state Raman features that manifest as positive peaks. The spline baselines drawn for all the excited-state FSRS spectra are shown in Figure S2 (from –1.5 ps to 600 ps) and Figure S3 (enlarged spectral region, from –100 fs to 1 ps) in the Supporting Information, and it is apparent that the transient absorption feature in this spectral region does not induce a large and time-dependent background to interference with the baseline drawing. The S_1 spectrum is fitted the same way as the S_0 spectrum, except that the S_1 vibrational features are generally broader due to shorter lifetimes. As a result, we plot the time-dependent center frequency of the consistently fitted gaussian peak in the kinetic analysis of each S_1 mode, as well as the integrated peak areas to better represent the intensities of the observed Raman modes. The least-squares multi-exponential fitting to the mode intensity kinetic traces is convoluted with the instrument cross-correlation time of ~140 fs.

III. Results

In order to unravel the primary photophysical and photochemical events of the GEM-GECO1 biosensor, we carried out static and ultrafast spectroscopic measurements on the Ca^{2+}-free and bound GEM-GECO1 proteins in aqueous buffer solution. Computational results based on density functional theory[60] are combined with spectroscopic data to ascertain

characteristic vibrational motions that facilitate or accompany ESPT in GEM-GECO1. Particularly, the direct observation of relatively low-frequency modes in the excited state between 400 and 800 cm^{-1} provides new insights into the initial stage along the ESPT reaction coordinate, regarding nuclear motions of the chromophore in the H-bonding network inside the protein pocket and intramolecular coupling between various vibrational motions.

A. UV/Vis and Fluorescence Spectroscopy

The electronic absorption and emission spectra of GEM-GECO1 protein samples with and without Ca^{2+} in aqueous buffer solution are measured and compared in Figure 1c (also see Figure S1 in the Supporting Information). The GEM-GECO1 protein has the same Ser-Tyr-Gly (SYG) chromophore as wtGFP[40,65] and exhibits similar absorption maximum at ~398 nm and green fluorescence at 512 nm in the absence of Ca^{2+}. Also, GEM-GECO1 shows no significant absorption near 476 nm, which is commonly assigned to the deprotonated chromophore (B state) that has a lower lying electronic excited state than the protonated chromophore (A state). Its singular absorption peak at ~400 nm thus corresponds to the A→A* (the first singlet excited state, S_1, of the protonated chromophore) transition, and the protonated chromophore is favored in both the Ca^{2+}-free and bound protein at the electronic ground state (S_0, see Figure 1c).[61] The dominant green fluorescence in the Ca^{2+}-free protein infers that A* converts to an excited intermediate deprotonated state (I*) via ESPT after 400 nm photoexcitation, and the I*→I transition of the chromophore emits redder to the A*→A transition.[39] The quantum yield for this large Stokes shift green fluorescence is 0.31, lower than 0.8 for wtGFP,[6,28] which we attribute to labile water molecules participating

in the ESPT chain and fluorescence quenching in the Ca^{2+}-free GEM-GECO1.[36,37]

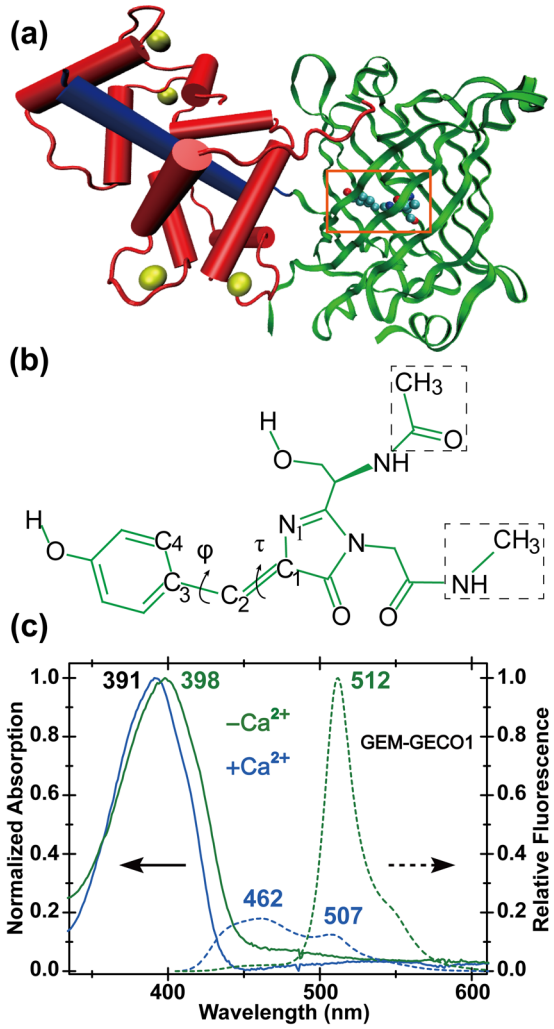

Figure 1. Illustrative structure of the GEM-GECO1 biosensor for Ca^{2+} imaging and its electronic spectroscopy results. (a) Protein structure of GEM-GECO1 in the Ca^{2+}-bound state as represented by the analogous GCaMP2 (PDB ID 3EVR)[36] with the circularly permutated GFP (cpGFP) β-barrel in green, the CaM domain in red, the M13 peptide in blue, and the calcium ions bound to CaM in yellow. The structure is rendered using VMD.[66] The embedded chromophore near the β-barrel opening is indicated by the orange box. (b) Molecular structure of the SYG chromophore. The methyl group of Thr223 is replaced by an H atom without further structural modification to obtain the SYG chromophore. The connections to the protein backbone are capped with CH_3CO at the N terminus and

$NHCH_3$ at the C terminus, respectively. The τ (N_1–C_1=C_2–C_3) and φ (C_1=C_2–C_3–C_4) dihedral angles are also shown. (c) Normalized UV/Vis absorption spectra of the Ca^{2+}-free (green solid curve, left axis) and Ca^{2+}-bound (blue solid curve) GEM-GECO1. The steady-state relative emission spectra of GEM-GECO1 (λ_{ex} = 400 nm) in the absence (green dashed curve, right axis) and presence (blue dashed curve) of Ca^{2+} show dramatic differences.

Upon Ca^{2+} binding to the remote CaM domain (Figure 1a), the absorption and emission maximum of the GEM-GECO1 chromophore blueshifts to ca. 391 and 462 nm, respectively, showing that the potential energy surface (PES) of the chromophore is modified in the excited state. The broader emission peak width in the Ca^{2+}-bound protein is likely due to the inhomogeneity of the chromophore local environment as large structural rearrangements occur after Ca^{2+} binding. The ~462 nm blue fluorescence of the Ca^{2+}-bound protein directly arises from the radiative decay of A*→A in the absence of ESPT. However, the small emission shoulder at ~507 nm is attributed to green fluorescence,[52,67] indicating that some ESPT still manages to occur in the Ca^{2+}-bound protein, which also corroborates the intrinsic inhomogeneity of the protein complex. Notably, the fluorescence intensity of the Ca^{2+}-bound protein is much weaker than that in the Ca^{2+}-free protein. This decrease of quantum yield (0.18, measured at the 455-nm emission peak)[28] argues that blue emission is competing with other nonradiative pathways to dissipate photoexcitation energy in the chromophore pocket.

B. Ground State and T=0 fs Excited State FSRS Spectra

As previously reported,[61] the ground-state Raman spectra of GEM-GECO1 without and

with Ca^{2+} are largely similar due to a primarily conserved protein pocket where the chromophore is embedded. The relatively low signal-to-noise ratio in Figure 2 could contribute to some observed spectral variations between the two protein samples. To illustrate the difference in electron redistribution over the chromophore after photoexcitation, we compare the Raman spectra of GEM-GECO1 both without and with Ca^{2+} in S_0 and S_1 at T=0 fs (Figure 2). The ground-state Raman spectra above 800 cm^{-1} are similar to our earlier work, which focused on the high-frequency region, i.e., ~800—1700 cm^{-1}.

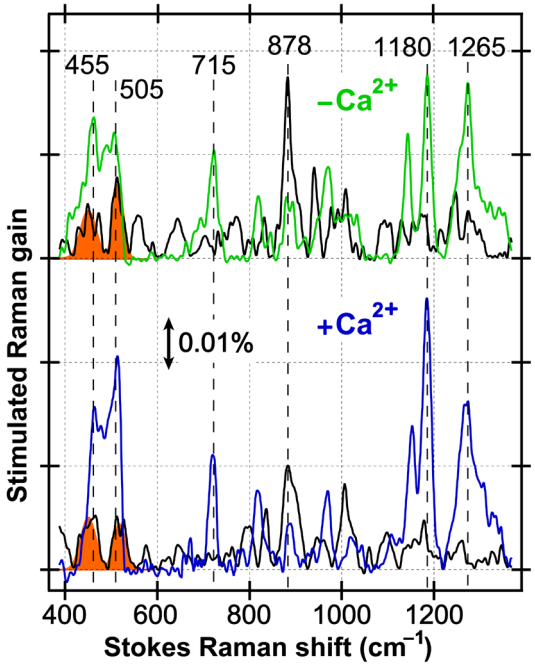

Figure 2. Comparison of the ground-state and T=0 fs excited-state FSRS spectra of the Ca^{2+}-free and bound GEM-GECO1. For the Ca^{2+}-free protein, the S_0 spectrum (black solid trace, upper panel) is overlaid with the S_1 spectrum at photoexcitation time zero (green solid trace). For the Ca^{2+}-bound protein in the lower panel, the S_0 and S_1 (T=0 fs) spectra at time zero are shown by the black and blue solid traces, respectively. Two marker bands below 600 cm^{-1} are shaded with orange gaussian-fitted peaks in S_0, which are greatly enhanced in S_1. Prominent vibrational modes are indicated by vertical

dashed lines with their frequencies labeled above. The double-arrowed black vertical line represents the absolute stimulated Raman gain strength of 0.01%. A rearranged version of this figure that directly overlays the two S_0 spectra (Ca^{2+} free vs. bound) and two S_1 spectra at T=0 fs (Ca^{2+} free vs. bound) for comparison is shown in Figure S4 in the Supporting Information.

For both the Ca^{2+}-free and bound proteins, the observed Raman signal in S_1 is stronger than S_0 even though we estimate (from the small dips corresponding to ground-state depletion in the time-resolved FSRS difference spectra) that only ~10% of the S_0 population converts to S_1 upon photoexcitation.[42,62] This result confirms the resonance enhancement effect because the 800 nm Raman pump pulse is close to a broad excited-state absorption peak of the SYG chromophore, which is at ~900 nm in wtGFP.[42] In contrast, the relatively weak S_0 spectrum is solely relying on two-photon absorption[6,68] to *enhance* the Raman scattering signal because the $S_0 \rightarrow S_1$ transition of the chromophore is at ~400 nm (Figure 1c). When comparing the S_0 spectra between two samples, we note that the peak intensities are generally larger in the Ca^{2+}-free protein than the Ca^{2+}-bound protein, consistent with higher concentration of the Ca^{2+}-free sample (estimates from the unnormalized electronic absorption spectra, see Figure S1 in the Supporting Information) that also has smaller molar extinction coefficient.[28] Upon photoexcitation, the S_1 spectral peaks in the Ca^{2+}-bound protein become stronger than those in the Ca^{2+}-free protein, which strongly argues that the resonance enhancement and/or enhanced Raman polarizability play a more significant role in the Ca^{2+}-bound protein. The implication for the loss of the chromophore two-ring coplanarity will be discussed later.

Previous research has reported Raman modes for the model chromophore and fluorescent

proteins,[42,69-71] but the low-frequency motions are much less studied while computational results are prevalent in the literature.[72-74] In this work, we focus on the excited-state vibrational motions below 800 cm^{-1}, including ca. 460, 504, and 715 cm^{-1} modes, mainly associated with ring in-plane deformation and ring-H out-of-plane (HOOP) wagging motions of the chromophore (Table 1). Following 400 nm photoexcitation, the Ca^{2+}-free/bound GEM-GECO1 exhibits noticeable changes in the low-frequency region: the 448/450 cm^{-1} S_0 mode promptly blueshifts to 455/465 cm^{-1}, the adjacent 507/509 cm^{-1} mode shows a slight redshift to 503/504 cm^{-1}, and the weaker 750 cm^{-1} mode redshifts to 715 cm^{-1}. All these lower frequency S_0 modes are greatly enhanced in S_1 (A* state), similar to the high-frequency modes, but the detailed mode kinetic analysis shows clear differences (see below).

C. Computational Results for the Vibrational Normal Modes in S_0 and S_1

Density functional theory (DFT) calculations are implemented to correlate specific molecular motions with the observed vibrational modes in the FSRS spectra. In the absence of a crystallographic structure for GEM-GECO1, the initial chromophore structure (Figure 1b) is constructed in the Gaussian 09 suite program.[60] We first perform DFT-B3LYP calculations with the 6-31G+(d, p) basis set on the S_0 chromophore *in vacuo* to resemble the hydrophobic protein pocket. The S_1 geometries are optimized by TD-DFT,[75,76] and the vibrational normal mode frequencies are deduced on the basis of optimized structures. The output geometries in S_0 after energy minimization yield nearly coplanar conformations between the phenol and imidazolinone rings (Table S1 in the Supporting Information), which support the π-conjugation across the ethylenic bridge of the double-ring chromophore. However, the

geometrically optimized structures in S_1 show some degree of twisting.[77,78] To approximate the excited-state I* structure, the same level calculations are conducted on the deprotonated chromophore (–1 charge, singlet) (Table S2). Detailed mode assignments for the observed vibrational modes are listed in Table 1, and depicted in Figure S5 in the Supporting Information. In particular, we find that the 448/450 and 507/509 cm^{-1} modes in S_0 have more OOP motions while the 750 cm^{-1} mode mainly involves in-plane imidazolinone ring deformation of the chromophore. It is consistent with the ground-state FSRS spectrum (Figure 2) showing stronger peak intensities for the two lower frequency modes because the Raman polarizability is typically larger for OOP motions.[55,79] This trend remains valid in S_1.

We also perform the same level of DFT calculations on the chromophore with twisted τ and φ dihedral angles as labeled in Figure 1b. It has been reported[80,81] that the GFP chromophore loses the π-conjugation between the phenol and imidazolinone rings when reaching S_1 (consistent with our calculation trend in Table S1), which allows the τ (exocyclic C=C bond torsion) and φ dihedral angles to rotate away from coplanarity. Most molecular mechanics calculations reveal that the τ and φ torsions proceed in opposite directions in a protein environment, e.g., a clockwise (+) τ twist and an anticlockwise (–) φ twist.[82,83] To understand the primary molecular geometry changes in our experiment, we twist the optimized structure of the chromophore from S_0 calculation and freeze the τ and φ dihedrals to various angles. DFT calculations are then performed in S_0 because most of the lower frequency collective motions have similar vibrational frequencies upon electronic excitation and the calculations can proceed more efficiently. Additional TD-DFT results are also obtained at three representative twisting geometries in S_1. As shown in Table S1, the

calculated lower frequency mode frequencies vary to some extent particularly for the 527 and 675 cm^{-1} modes. Notably, these frequencies are obtained for the geometrically optimized chromophore structure *in vacuo* in S_1, which cannot be quantitatively compared to the initial stage (e.g., <200 fs) FSRS mode frequencies of the chromophore in the protein pocket following photoexcitation. This is because even though electronic redistribution occurs promptly, the chromophore does not have enough time to equilibrate in S_1 on that ultrafast timescale so its nuclear coordinates still largely resemble those in S_0. The trend of mode frequency change is the important parameter we use to correlate with experimental observations at later time (i.e., on the sub-ps to ps timescale).

D. Time-Resolved Excited-State FSRS Spectra Before Fluorescence

The time-dependent FSRS spectra are presented in Figure 3 as a stacked plot, providing a vivid molecular movie about the excited-state conformational dynamics of the Ca^{2+}-sensing CaM-GFP complex. The focus here is on the prominent lower frequency modes of GEM-GECO1 and how they respond to Ca^{2+} in the photoexcited state. Markedly, the excited-state FSRS spectra of the Ca^{2+}-free and bound GEM-GECO1 exhibit an array of positive features immediately following 400 nm photoexcitation. These vibrational features in the ca. 800—1350 cm^{-1} spectral region, highlighted by the red rectangle, are consistent with the FSRS data we collected within a spectral window from ca. 800—1700 cm^{-1} albeit with slight differences in the mode intensities.[61] The FSRS peak intensity scales linearly with the number of Raman probe photons[62,84-86] but the stimulated Raman gain should in principle be independent from the probe intensity (see Supporting Information). The prominent peaks

at ca. 455/465, 505/506, and 715/715 cm^{-1}, labeled in the green/blue box for the Ca^{2+}-free/bound protein (Figure 3) up to 600 ps, all emerge promptly (within the cross-correlation time of ~140 fs) together with the higher frequency Raman modes (see Figures S6–S8 for representative intensity kinetic plots) following photoexcitation. The intensities for all the excited-state vibrational modes are comparable to if not higher than those in S_0 because of the resonance enhancement for the S_1 Raman features.

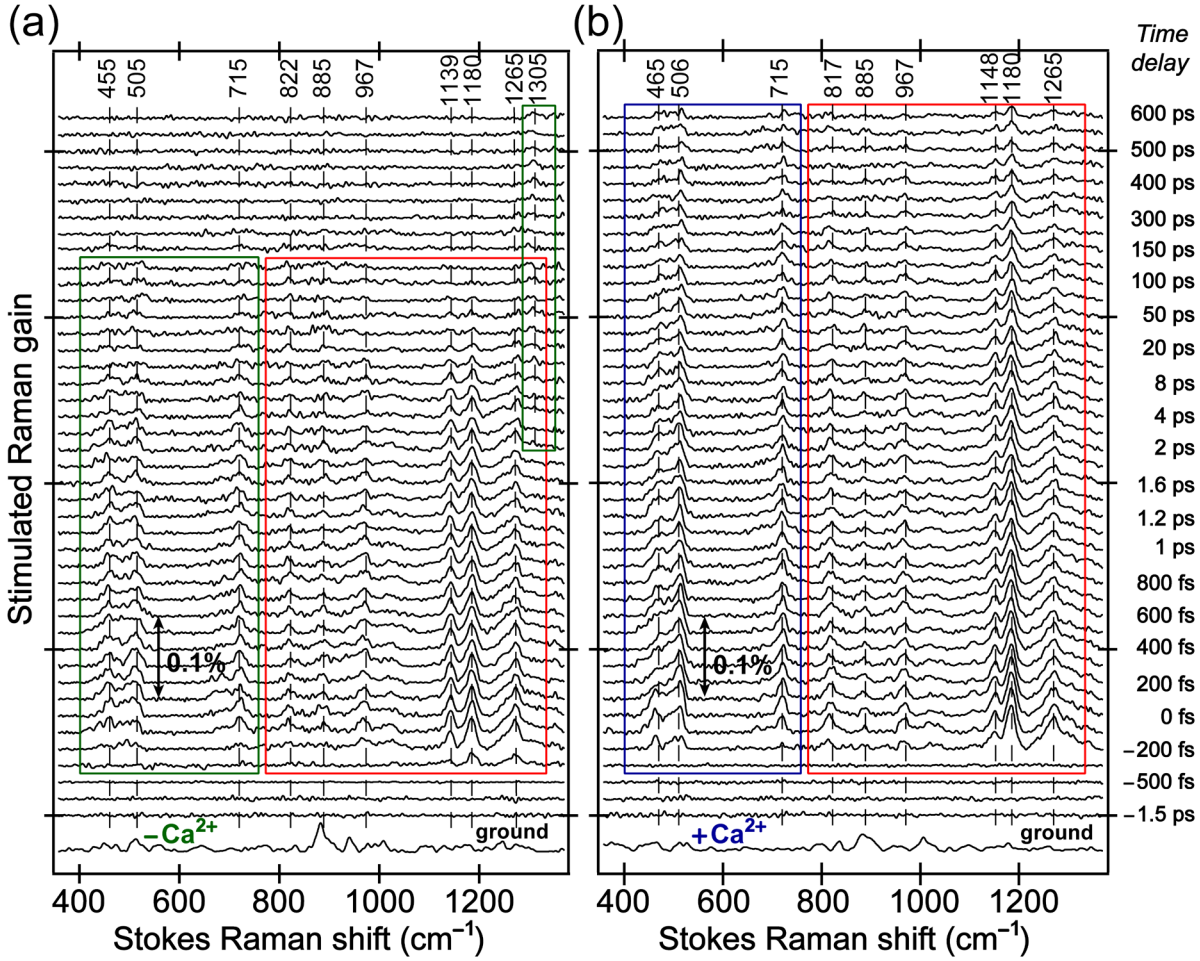

Figure 3. Time-resolved excited-state FSRS spectra of both (a) Ca^{2+}-free and (b) Ca^{2+}-bound GEM-GECO1 from –1.5 to 600 ps following 400 nm photoexcitation. The Raman pump is centered at 802 nm. The buffer-removed ground-state FSRS spectra of the proteins are plotted at the bottom for

comparison within a spectral window of ca. 350—1400 cm^{-1}. Every other time delay between the fs photoexcitation and Raman probe pulses is labeled on the right side of the spectra. Not all the time points are shown. The two red boxes enclose the high-frequency ($>$800 cm^{-1}) modes, while the large green/blue box in the Ca^{2+}-free/bound spectra emphasizes the lower frequency modes. The small green rectangle in the upper right corner of (a) highlights the 1305 cm^{-1} mode of I* in the Ca^{2+}-free protein. The center frequency of the prominent S_1 modes throughout the detection time window is labeled on the top. The absolute Raman gain strength of 0.1% is shown with the double-headed arrow.

The most striking difference between Figure 3a and 3b lies in the vibrational peak evolution. In the Ca^{2+}-free protein, the modes associated with the chromophore A* state all show rapid decay while the 1305 cm^{-1} mode rises with the formation of the deprotonated I* state.[42,61] However, in the Ca^{2+}-bound protein, all modes across the detection window persist throughout the entire 650-ps observation time frame (limited by the 100-mm linear translation stage in our experimental setup), indicating that ESPT is hindered and the chromophore A* state directly emits blue fluorescence (see below for discussion).

E. Dynamics of the Excited-State Low-Frequency Vibrational Modes

To obtain the ultrafast dynamics of the collective skeletal modes for the GEM-GECO1 chromophore, we perform the least-squares fitting to the time-resolved traces for three marker bands below 800 cm^{-1} (see Figure 3). Peak assignments are made on the basis of computational results for S_1 modes (Table 1). Figure 4 shows the kinetic plots of three marker bands in both protein samples. The ultrafast rising component for the mode intensities is

within the ~140 fs cross-correlation time between the actinic pump and Raman probe pulses. For the 455/465 cm^{-1} mode in Figure 4a, both samples show similar initial decay time constant, ~1.3/1.4 ps for the Ca^{2+}-free/bound protein, respectively. This stage corresponds to the chromophore moving out the FC region without significant nuclear motions,[42] while the photoexcited wavepacket moves toward the lower portion of excited state (S_1) PES.

In contrast, the second decay component shows dramatic change upon Ca^{2+} binding, with the time constant of 45/410 ps for the Ca^{2+}-free/bound protein (i.e., for the ~460 cm^{-1} mode), respectively. The 45 ps time constant is slightly longer than the previously reported time constant of ~30 ps attributed to ESPT in the Ca^{2+}-free biosensor, derived from the kinetic analysis of high-frequency modes, i.e., >1000 cm^{-1}.[61] This result argues that the collective skeletal motions take more time than largely localized modes to respond to the A*→I* conversion and population changes as ESPT proceeds in the Ca^{2+}-free GEM-GECO1, with a mostly coplanar chromophore. In contrast, the much longer second decay time constant for the Ca^{2+}-bound protein suggests the inhibition of ESPT and existence of some nonradiative relaxation pathways, which may compete with blue fluorescence directly from the A* state.[46,64,67] It is interesting to note that the second decay time constants are actually shorter in the 465 and 504 cm^{-1} modes than the other higher frequency modes in the Ca^{2+}-bound protein. This reversed trend is likely correlated with the fact that in the absence of ESPT, the more twisted chromophore administers a faster decay of the collective skeletal motions within a trapped A* state due to their increased sensitivity to the electronic polarizability change and curvature of the excited-state PES.[87,88]

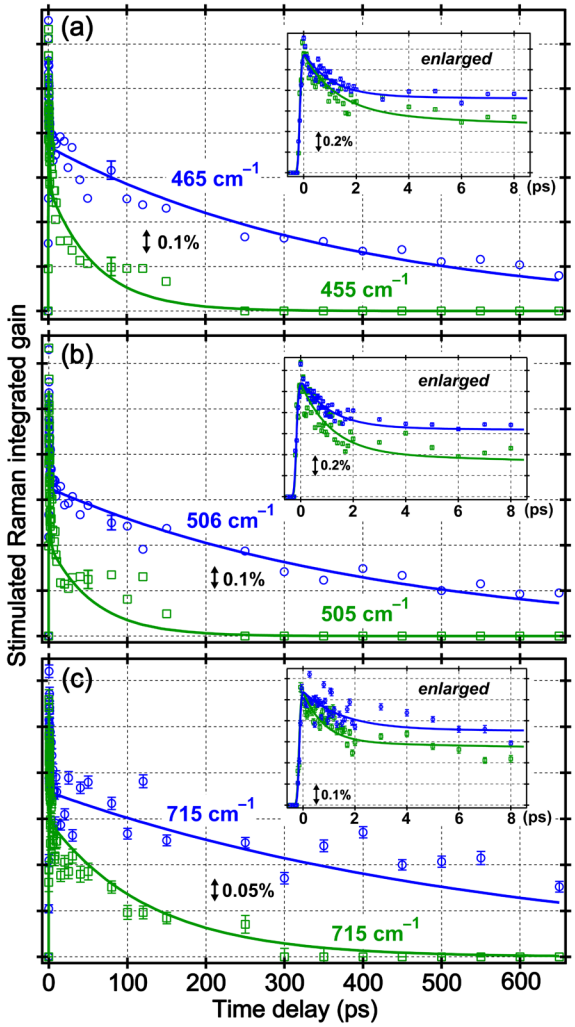

Figure 4. Time evolution of three relatively low frequency excited-state Raman modes in the Ca^{2+}-free and bound GEM-GECO1 shows distinct pattern. Intensity kinetic plots of modes at (a) 455 and 465 cm^{-1}, (b) 505 and 506 cm^{-1}, and (c) 715 and 715 cm^{-1} for the Ca^{2+}-free (green) and bound (blue) proteins, respectively, in aqueous buffer solution following 400 nm photoexcitation up to 650 ps. All the modes in both protein samples show double exponential decay (fits are shown in solid lines, and the experimental time zero retrieved from least-squares fitting is ca. –150 fs), but the second decay time for the Ca^{2+}-bound protein is much longer than that for the Ca^{2+}-free protein. The enlarged dynamics plot within 8 ps exhibits a similar initial relaxation phase (< 2 ps decay time constant, see Table 1) regardless of Ca^{2+} binding (shown in the insets). The typical error bars (one standard

deviation of the gaussian-fitted peak area, at least three independent data sets) are shown for one time delay point in (a) and (b), and for all the data points in (c) where the peak intensity is weaker. The absolute magnitude of the Raman integrated gain is noted in each subfigure as the vertical double-arrowed line. The apparent larger spread of data points in the insert of (c) is due to mode intensity quantum beating (Figure S6) on the sub-ps to ps timescale.

All three vibrational modes in S_1 below 800 cm^{-1} manifest a biphasic exponential decay (Figure 4) with time constants listed in Table 1. The dynamics similarity is correlated with the fact that these modes represent delocalized skeletal motions. The components of phenol ring HOOP and hydroxyl rocking for the 460 cm^{-1} mode are closely related to the phenolic proton motions of the chromophore, so its high sensitivity to the proton-coupled electronic redistribution may contribute to its relatively faster relaxation. In contrast, the slightly longer decay time constants of the 504 cm^{-1} mode are consistent with its assignment of involving more ethylenic-bridge HOOP motions. The inclusion of serine sidechain O–H wagging in the 504 cm^{-1} mode implies that the chromophore motions are not limited to the phenolic end to search phase space for ESPT, instead, the other end of the proposed ESPT chain in the protein pocket also experiences ultrafast conformational changes and may accompany ESPT in a concerted manner.[39,53,65,89,90]

Figure 4c presents the kinetic plot of the 715 cm^{-1} mode in S_1, which involves strong imidazolinone-ring deformation, bridge CH motion, and phenol ring-H rocking (Table 1). The biexponential decay time constants are 1.8/2.0 and 120/670 ps for the Ca^{2+}-free/bound protein. The much longer decay time constants in comparison to those for modes below 600

cm^{-1} are likely due to the nature of the normal mode involving more imidazolinone ring motions. It is known that the primary ESPT step initially involves the departure of the phenolic proton, and the increasing negative charge on the phenolic hydroxyl oxygen atom transfers back to the aromatic ring system (i.e., the phenolic ring, then the imidazolinone ring).[91,92] The 715 cm^{-1} mode may also survive the ESPT barrier crossing to a larger extent and show similar frequency in the I* state, leading to an apparently lengthened decay. Interestingly, calculation results (Table S2) indeed show little frequency difference (4 cm^{-1}) for this mode between the protonated and deprotonated chromophore in S_1.

Notably, the 715 cm^{-1} mode exhibits spectral oscillations (quantum beats) within 2 ps following photoexcitation. The involvement of bridge CH motions may contribute to the sensitivity of the mode polarizability to electronic redistribution over the two-ring system. In the Ca^{2+}-free protein, the mode intensity manifests an oscillatory pattern with a reproducible period of ~200 fs (Figure S6). Discrete Fourier transform (DiFT) is performed on the coherent oscillatory residual after removing the incoherent rise and decay component. A dominant ~175 cm^{-1} peak is revealed, corresponding to an in-plane phenol-ring rocking motion about the bridge carbon corroborated by TD-DFT calculations. Our previous observation of the oscillatory 819, 885, and 967 cm^{-1} modes lends further support to this viewpoint as they also involve ethylenic bridge motions.[61] In the presence of Ca^{2+}, the observed mode oscillation does not have one constant period. The DiFT result exhibits several underlying modulation modes between 100—300 cm^{-1} with approximately equal intensity, suggesting that the anharmonic coupling matrix between these vibrational modes[93-95] on the S_1 PES changes in response to Ca^{2+} binding at the CaM domain.

An interesting finding is that the 455 and 503 cm^{-1} modes in the Ca^{2+}-free protein do not exhibit significant spectral oscillations within the first 2 ps, indicative of a complex anharmonic coupling matrix in which not all the vibrational modes are effectively modulated by one dominant low-frequency mode.[96] We consider that the weak coupling between certain vibrational modes is governed by the local environment and the nature of pertaining atomic motions. For instance, the involvement of phenolic hydroxyl rocking in the 455 cm^{-1} mode makes it less sensitive to the phenolic ring rocking, while the concentration of the 503 cm^{-1} mode on the serine hydroxyl on the opposite ring diminishes its correlation to the phenolic rocking motions. FSRS results on another related GECO protein biosensor G-GECO1.1 that is intensiometric[28] show similar results of diminished spectral oscillations, which will be discussed in a future publication.

One of the advantages of exploiting FSRS to elucidate photochemical events is the simultaneous observation of a wide array of transient vibrational modes in one data scan, afforded by the fs Raman probe pulse generated from supercontinuum white light.[44,84,97,98] With the focus on the lower frequency modes, we still observe the high-frequency marker bands within the broad spectral window and they offer desirable consistency to track photochemical reactions at the molecular level. The kinetic plots for two excited-state vibrational modes at 1180 and 1265 cm^{-1} are presented in the Supporting Information, Figures S7 and S8, respectively. They show similar biexponential decay time constants as those in our previous report,[61] and clear intensity quantum beats in the Ca^{2+}-free protein that arise from the dominant modulation mode at ~175 cm^{-1} (Figure S8).

F. Initial Frequency Blueshift of Two Vibrational Marker Bands in S_1

What are the primary structural events in the A* state of the chromophore before ESPT? A close inspection of the two marker bands at ~460 and 504 cm^{-1} in the first 1.5 ps following photoexcitation reveals characteristic frequency evolution (Figure 5). In Figure 5a, we note that the mode frequency is initially lower (by ~15 cm^{-1}) in the Ca^{2+}-free than Ca^{2+}-bound protein. This observation is due to the mode composition involving collective motions on the phenol ring as well as the phenolic hydroxyl (COH) rocking, so a more hydrophilic environment such as the Ca^{2+}-free protein pocket with labile water molecules supports more H-bonding and electron delocalization: the mode frequency becomes lower.[99,100] Moreover, the Ca^{2+}-bound protein shows a mode frequency blueshift from 458 to 466 cm^{-1} as the delay time changes from –200 fs to 1.5 ps, while the Ca^{2+}-free protein shows a larger blueshift from 443 to 456 cm^{-1}. The smaller blueshift observed for the Ca^{2+}-bound (8 cm^{-1}) than the Ca^{2+}-free protein (13 cm^{-1}) is indicative of a more compact environment as the chromophore initially evolves on the S_1 PES with Ca^{2+}. A single exponential fit to the data traces yields ca. 210/140 fs time constant for the mode blueshift in the Ca^{2+}-free/bound chromophore.

This dynamic timescale is intriguing because (1) it is fast compared to the vibrational period of skeletal motions (e.g., a 170 cm^{-1} mode corresponds to a vibrational period of ~200 fs) and the frequency shows a monotonic change, so skeletal periodic motions cannot be the dominant cause; (2) it is fast in comparison to typical intra- or inter-molecular vibrational energy redistribution on the ps timescale;[101-103] and (3) it is too slow for the electronic redistribution upon photoexcitation that typically occurs on the attosecond to femtosecond timescale.[104-107] A logical explanation for this ultrafast time constant is pertaining to the

initial proton movement along pre-existing H-bonding chains, which typically occurs on the 100 fs timescale (discussed in detail below).[108-111]

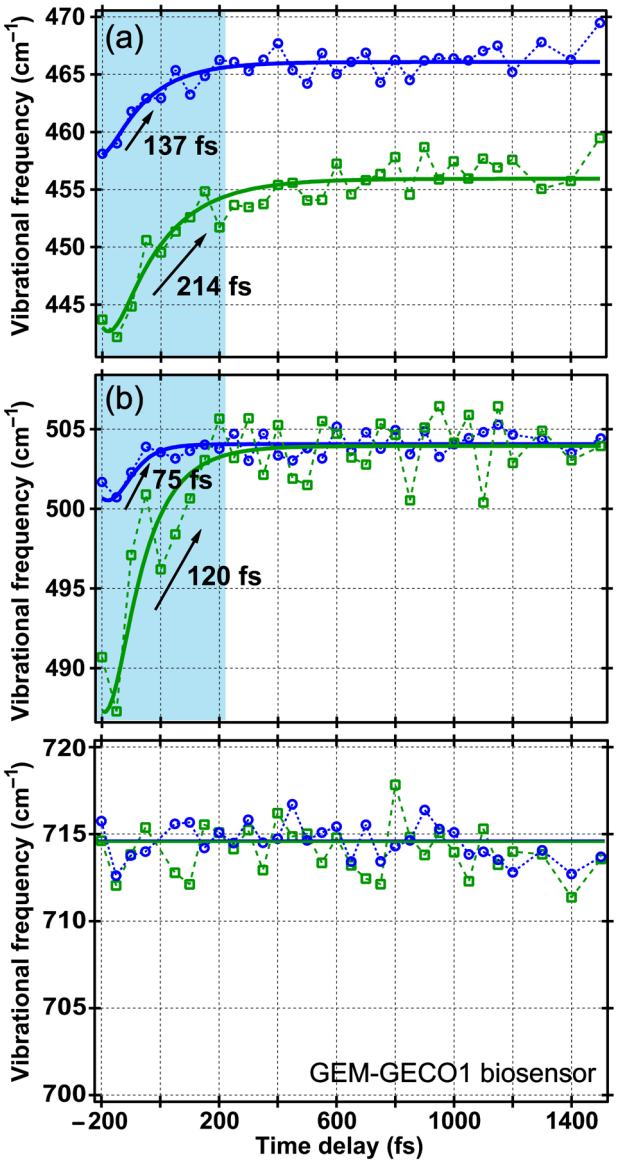

Figure 5. Initial stage of the frequency evolution of three lower frequency excited-state vibrational modes. Kinetic plots of the center frequencies of modes at (a) 455/465 cm^{-1}, (b) 503/504 cm^{-1}, and (c) 715/715 cm^{-1} for the Ca^{2+}-free (green)/bound (blue) GEM-GECO1 following 400 nm photoexcitation up to 1.5 ps. The two modes below 550 cm^{-1} manifest a single-exponential blueshift from ca. –200 fs to 200 fs in (a) and (b), highlighted by the shaded light blue rectangle with the blueshift time constants

labeled therein. Considering the experimental time zero is ca. –150 fs from intensity least-squares fitting (Figure 4), the mode frequency starts to shift from ca. –50 fs that is consistent with the Raman probe pulse duration. The modes in the Ca^{2+}-bound protein exhibit a relatively faster blueshift and a smaller frequency change than those in the Ca^{2+}-free protein. In contrast, within the same time period, the 715 cm^{-1} mode in (c) shows a largely conserved frequency within experimental error, regardless of Ca^{2+} binding, denoted as a straight line through the data points.

Figure 5b presents the kinetic data of the mode with the average (from –100 fs to 1 ps) frequency of 503/504 cm^{-1} for the Ca^{2+}-free/bound protein, which displays a blueshift time constant of ca. 120/75 fs, both within the cross-correlation time. Though the Ca^{2+}-free protein still displays a lower frequency initially, its difference from the Ca^{2+}-bound protein (~10 cm^{-1}) is less than the 460 cm^{-1} mode case (Figure 5a). The assignment of the 504 cm^{-1} mode (Table 1 and Figure S5) involves bridge-HOOP and serine sidechain O–H wagging motions, which is farther away from the phenolic ring where the ~460 cm^{-1} mode is concentrated. Therefore, the *faster* blueshift of the 504 cm^{-1} mode is inconsistent with the picture of coherent proton motions only occurring at the phenolic hydroxyl end. In addition, the *smaller* magnitude of the mode blueshift is likely due to the mode composition with more imidazolinone ring contributions (see Supporting Information), because the photoexcited coherent proton motions at this end of the ESPT chain may be smaller in scale than the phenolic proton motions (i.e., the 460 cm^{-1} mode involves the phenolic hydroxyl in-plane rocking).

We also analyze the frequency evolution of the 715 cm^{-1} mode within the initial ~2 ps, which evinces small oscillations but without marked blueshift or redshift (Figure 5c). We

surmise that this collective imidazolinone-ring deformation mode coupled with bridge CH motions is less sensitive to the charge transfer following initial coherent photon motions at both the phenol hydroxyl and serine sidechain hydroxyl end. Some cancellation effect may help explain the unchanged mode frequency in S_1. This mode displays a noticeable blueshift if ring twisting occurs in S_1 (Table S1) that is *not* observed in the experimental data, consistent with the restraint exerted by the protein matrix on the chromophore.

IV. Discussion

Due to the technical challenge of using long-wavelength IR pulses or the weak Raman scattering signals from conventional Raman, the low-frequency vibrational modes of a protein chromophore remain an underexplored subject.[53,112-114] However, a detailed understanding of the functional role of skeletal motions that typically involve delocalized electrons and multiple atoms is instrumental to dissect the excited-state multidimensional PES and map the photochemical reaction coordinate leading to radiative/non-radiative relaxation. The question regarding the fluorescence modulation mechanism of this newly developed dual-emission Ca^{2+}-sensor GEM-GECO1,[28] really comes down to the role of characteristic atomic motions of the chromophore prior to and during ESPT. These motions are intimately correlated with the protein pocket that hosts the chromophore, which is essentially the active site of the biosensor that determines its macroscopic functionality.

The main contribution of this work is the time-resolved analysis of a number of low-frequency vibrational modes of the chromophore inside a protein biosensor. In contrast to extensive literature studying fluorescent proteins in the electronic domain,[39,45-49,115-117] the

results obtained using FSRS are unique because the pure excited-state vibrational motions can be revealed, while the signal-to-noise ratio is greatly improved due to resonance enhancement of S_1 going to a higher lying electronic state (e.g., S_2) with a suitable Raman pump. We capture the transient dynamics of lower frequency modes at ca. 460 and 504 cm^{-1} in addition to the 715 cm^{-1} mode (Figures 3–5, and Figure S6 in the Supporting Information), together with temporal evolution of the high-frequency vibrational modes (Figures 3, S7, and S8). They are potentially modulated by the impulsively excited low-frequency modes below 300 cm^{-1} in S_1, enabled by the bandwidth of the ~40 fs photoexcitation pulse. These new results provide a more complete picture of ESPT in GEM-GECO1 starting from time zero of photoexcitation and evolving toward different fluorescent states, depending upon whether or not Ca^{2+} is allosterically bound to the CaM domain (Figure 1a).

A. Evidence of a More Twisted Chromophore in the Ca^{2+}-Bound Protein Biosensor

From UV/Vis spectral analysis, the peak absorption of the Ca^{2+}-free GEM-GECO1 at 398 nm represents a redshift from the Ca^{2+}-bound protein peak at 391 nm (Figure 1c), revealing a larger energy gap between S_0 and S_1 upon Ca^{2+} binding to the CaM domain. For the GCaMP family of proteins, the CaM domain wraps around the M13 peptide upon Ca^{2+} binding (Figure 1a), occluding the GFP β-barrel opening and changing the chromophore environment.[28,36,37,61,118] In GEM-GECO1, structural rearrangement pushes several bulky and hydrophobic residues toward the existing H-bonding network around the chromophore,[28] disrupting its ESPT capabilities. In particular, Pro377 in the CaM domain close to the GFP interface likely repositions nearby methionine residues (e.g., M374, M375, and/or M379) to

increase the hydrophobicity of the GFP pocket. This different protein matrix exerts some strain on the chromophore, causing slight deviations from coplanarity that disrupt its π-electron delocalization across the two rings.[83] A more twisted chromophore structure is thus expected for the Ca^{2+}-bound protein in S_0, and the destabilization energy for S_1 is more than that for S_0 owing to the photoacidity of the chromophore as well as a combination of steric, electrostatic, and specific interactions within the protein pocket.[119] The evidence also appears in the FSRS spectra (Figure 2). Though the Ca^{2+}-bound protein has slightly weaker Raman intensity in S_0 due to lower concentration (Figure S1), it actually shows stronger intensity than the Ca^{2+}-free protein in S_1 at photoexcitation time zero. This intensity increase can be explained by the higher Raman polarizability in a more twisted, non-equilibrium chromophore structure in the photoexcited Ca^{2+}-bound protein. Since it is the S_1 Raman spectra at T=0 fs and no significant atomic motions are expected to occur, the twisted structure of the chromophore two-ring system should already exist in S_0.

Following 400 nm photoexcitation, will this twisted chromophore undergo further torsion or revert back to a coplanar conformation to undergo ESPT? This type of structural dynamics insights should be retrievable from the frequency evolution of the low-frequency vibrational modes of the photoexcited chromophore. We first compare the FSRS spectrum in S_0 vs. S_1 (T=0 fs): the 448/450 cm^{-1} mode blueshifts to 455/465 cm^{-1} in Ca^{2+}-free/bound proteins, and the close resemblance of the blueshift indicates that the chromophore undergoes similar electronic redistribution upon photoexcitation. The lower average frequency for this mode in the Ca^{2+}-free vs. bound protein suggests that the phenolic hydroxyl proton is in a more H-bonding environment without Ca^{2+} binding, hence leading to a more deprotonated

chromophore in the excited state (Table S2). In contrast, the nearby 504 cm^{-1} mode does not show significant frequency shift from S_0 to S_1, and it also displays a smaller magnitude of the initial mode blueshift in S_1 (Figure 5b). This observation indicates that the photoinduced electronic redistribution exerts less influence on the bridge HOOP and serine sidechain OH motion in comparison to the more phenol-ring-concentrated mode at lower frequency. Moreover, the ultrafast frequency shift recorded on the <200 fs timescale (Figure 5) is associated with the small-scale coherent proton movement through low-barrier H-bonds, without major structural rearrangement that occurs on a significantly longer timescale.[120] This process is likely accompanied by the onset of other low-frequency skeletal motions, which modulate the conformation of the chromophore including its H-bonding network with surrounding solvent molecules and protein residues to dissipate photoexcitation energy.[42,79]

Following the aforementioned initial mode blueshift within ~200 fs, these vibrational marker bands do not exhibit additional frequency shift (Figures 3 and 5), suggesting that the chromophore does not further twist in S_1 in comparison to S_0. The TD-DFT calculation results lend support to this point, as shown in Table S1 for the observed 715 cm^{-1} mode, its frequency increases by ~13 cm^{-1} in the hula-twisted chromophore[22,46,82,121] ($\tau = 20^{\circ}$ and $\varphi = -20^{\circ}$) than that in the excited-state coplanar chromophore. One of the extreme cases for such twisting is the *cis-trans* isomerization of the GFP model chromophore in solution, which renders the chromophore non-fluorescent.[89,122] In contrast, it is reasonable to consider the protein matrix favorable for tuning the S_1 PES of the chromophore to make it fluoresce efficiently, while disallowing large torsional motions due to steric hindrance. A recent report shows that upon chemical modification to conformationally lock a GFP-like synthetic

chromophore, the ring coplanarity is maintained that effectively suppresses the photoisomerization-induced deactivation, leading to photolytic dissociation.[123]

The observation of a more twisted chromophore conformation in S_0 and S_1 with Ca^{2+} provides a solid basis for understanding the dual-emission behavior of the GEM-GECO1 biosensor. In addition to the more hydrophobic environment created by pushing in hydrophobic/non-polar residues and reducing water molecules from the protein pocket, the twisted chromophore may have difficulty aligning with the few remaining and less mobile proton acceptors such as H_2O (vs. the Ca^{2+}-free case). The significant increase of the ESPT barrier will trap the twisted chromophore in A* after its initial wavepacket moves out of the FC region, which involves small-scale proton motions at both ends of the chromophore, but without the subsequent large-scale proton transfer via a coordinating ESPT chain.

B. Multi-Staged Structural Evolution of the Chromophore prior to ESPT

Upon 400 nm fs laser irradiation, the chromophore undergoes vertical excitation and electronic redistribution promptly, entering a non-equilibrium state that evolves in S_1. The FC dynamics then dominate the initial wavepacket motions, leading to the ultrafast blueshift of the observed lower frequency modes in both Ca^{2+}-free/bound proteins as seen in Figure 5. This suggests that the chromophore in S_1 initially undergoes coherent proton motion that induces charge transfer, a phenomenon characteristic of the photoacidity of the chromophore with phenolic hydroxyl groups.[91,92,124] Concerted electron-proton transfer has been observed for H-bonded dyes in the optical intramolecular charge transfer excitation using transient absorption techniques.[125] In our system, the GFP chromophore in the optically populated

locally excited state (LE, $^1\pi\pi^*$ characteristics) can efficiently transition into an energetically close charge transfer state (CT, $^1\pi\sigma^*$ characteristics)[81,126] on the ~100 fs timescale by involving small-scale proton motions.[108] This transition may strongly affect the 460 cm^{-1} mode dynamics because it mainly involves phenol ring motions that are closer to the phenolic hydroxyl end, accompanied by charge transfer from the hydroxyl oxygen toward the conjugated ring system.[91,125] The larger blueshift amplitude for the Ca^{2+}-free (~13 cm^{-1}) than the Ca^{2+}-bound protein (~8 cm^{-1}) indicates that the coherent proton motion in S_1 has a larger magnitude in the Ca^{2+}-free construct, consistent with the fact that GEM-GECO1 without Ca^{2+} has more CT characteristics in its specific protein environment, capable of undergoing ESPT on the ps timescale to reach the green fluorescent state.

It is notable that although the Ca^{2+}-bound protein emits blue fluorescence with ESPT inhibition, its chromophore is still in a H-bonding network in S_0 as evinced by the similarity of the UV/Vis spectrum and ground-state FSRS spectrum between the Ca^{2+}-free and bound proteins. The initial proton motion is expected to occur in a pre-existing H-bonding chain of both proteins, away from the chromophore and toward the proton acceptor(s). Such ultrafast proton motions have been observed in proton-coupled electron transfer reactions that manifest non-equilibrium dynamics where the traditional Born-Oppenheimer separation between electronic and nuclear motions may break down for light-mass hydrogen nuclei.[125,127] Moreover, the insensitivity of this early-stage proton motion promptly following photoexcitation to the subsequent difference in energy dissipation pathways attests the necessity to distinguish between the chromophore photoacidity and ESPT capability. The propensity of a photoacidic chromophore to push away a proton is an intrinsic molecular

property in S_1, no matter the local environment supports it or not. This is corroborated by our previous observation of the formation of a transient pyranine-methanol complex in S_1 with proton shuttling motions[64] despite the hindrance of ESPT. In contrast, the ESPT process intimately involves contributions from surrounding molecules which, depending upon the strengths and flexibilities of proton donors and acceptors, manifest as observable spectral features on a multitude of ultrafast timescales from fs to hundreds of ps.[42,62-64,105,108,128-139]

Interestingly, the 504 cm^{-1} mode does not involve the phenolic hydroxyl motions, but it exhibits a frequency blueshift on a faster timescale (~100 fs) than the 460 cm^{-1} mode (~170 fs). This result strongly argues against a picture of proton motions solely occurring at the phenolic hydroxyl end because that will lead to a slower response time for the 504 cm^{-1} mode to exhibit clear frequency shift. A logical explanation is that the serine sidechain hydroxyl closer to the imidazolinone moiety also undergoes coherent proton motion upon photoexcitation. The resultant 504 cm^{-1} mode blueshift shows faster dynamics than the 460 cm^{-1} mode in both Ca^{2+}-free/bound proteins (Figure 5), which reflects the influence of the surrounding protein environment on the chromophore motions starting from time zero.

This ultrafast stage of S_1 vibrational mode frequency shift is a new observation in this work. In the previous FSRS data on wtGFP,[42] frequency oscillations of two high-frequency (e.g., ~1262 and 1565 cm^{-1}) modes were observed on the sub-ps timescale, but there was no obvious mode frequency shift within the first ~200 fs. It is understandable that small-scale coherent proton motions may affect the low-frequency (<600 cm^{-1}) and high-frequency (>1000 cm^{-1}) modes in different ways, however, the 1262 cm^{-1} mode was assigned to the phenolic C–O stretch and it is hard to argue that its frequency is insensitive to phenolic

proton motions. From crystal structures of wtGFP,[40,41,65] the phenolic hydroxyl forms a H-bond with a conserved H_2O molecule located above and to one side of the phenol ring, which restricts the onset of ESPT along a ring-wagging-mediated reaction coordinate.[42] In GEM-GECO1, there is no conserved H_2O molecule around the phenolic hydroxyl end due to the β-barrel opening, indicative of a more flexible H-bonding network between the chromophore and protein matrix. The DiFT analysis of the 715 cm^{-1} mode intensity oscillations as well as molecular dynamics simulation results[61] all support that the initial ESPT in the Ca^{2+}-free GEM-GECO1 is along a phenol ring rocking coordinate. Consequently, the reduced transition barrier for the *initial* largely in-plane proton transfer leads to a distinct reaction stage that phenolic proton moves along the pre-existing H-bonding chain, in concert with the serine sidechain hydroxyl proton motions on the sub-200 fs timescale. While this photoacidity-dominant phase is rapidly over, a coherent low-frequency mode (i.e., ~175 cm^{-1}) works to facilitate ESPT on the hundreds of fs to a few ps timescale (Table 1, Figures S6 and S8) before the impulsively excited vibrational coherence decays away.

In contrast, immediately following photoexcitation that redistributes the electrons over the conjugated chromophore in wtGFP, the relatively large reaction barrier to transfer the phenolic proton to an out-of-plane H_2O acceptor hinders a distinct initial stage for proton motion. Rather, the photoinduced coherent low-frequency motions kick in promptly to search phase space and optimize the relative geometry between the phenolic hydroxyl and surrounding proton acceptors. Once the ESPT chain involving the conserved H_2O molecule and nearby heavy atoms such as serine and glutamic acid is optimized, proton transfer occurs efficiently over larger distances in the wtGFP pocket on the ~5 ps timescale.[42]

C. Effect of Protein Environment on the ESPT Capability of GEM-GECO1 Biosensor

The time-resolved FSRS measurement provides direct visualization of the dramatic effect of varied protein environment on ESPT processes responsible for the fluorescence modulation. For the Ca^{2+}-free protein, all lower frequency marker bands promptly emerge after photoexcitation and decay away within ~150 ps (Figures 3 and 4), indicating that ESPT is the primary pathway to release photoexcitation energy and an intermediate deprotonated chromophore emits green. In the Ca^{2+}-bound protein, the same vibrational modes persist over the entire detection time window of 650 ps, revealing the absence of ESPT so blue fluorescence from the A*→A transition dominates (Figure 1c).

In comparison to the reported high-frequency modes for both Ca^{2+}-free and bound proteins,[61] the dynamics for the three marker bands in this work exhibit longer decay time constants. This is because the lower frequency modes involve more ring deformation motions and their collective nature leads to slower evolution of nonlinear Raman polarizability. From the mode composition in Table 1 and Figure S5, we find the 715 cm^{-1} mode to be mainly associated with the imidazolinone ring in-plane deformation and bridge CH motions, while the 460 and 504 cm^{-1} modes largely involve HOOP motions on the phenol ring. The longer decay time constants for the former mode than the latter modes are thus indicative of more electronic and conformational changes at the phenol ring than the imidazolinone ring, and more proton transfer motions at the phenolic end than the other end of the chromophore. It is also notable that ESPT in the Ca^{2+}-free protein is accompanied by the motions of surrounding heavy atoms such as protein residues along the ESPT chain. They need to rearrange to accommodate a conformationally varying but still largely coplanar chromophore, which can

take tens of ps to transfer the proton in condensed phase.[42,129,140] However, the Ca^{2+}-induced change of the protein pocket conformational and electrostatic phase space dictates that the second decay time constants observed for the Ca^{2+}-bound protein are much longer than the Ca^{2+}-free protein (Table 1). This can be attributed to a much increased barrier to I* so the trapping at A* leads to blue fluorescence. A detailed discussion on the GEM-GECO1 fluorescence modulation mechanism with a series of site-specific mutagenesis results and molecular dynamics simulations can be found in our earlier report.[61]

After the initial proton motion in the first sub-200 fs, we observe the intensity oscillation of the 715 cm^{-1} mode in Ca^{2+}-free and bound proteins (Figure S6). The DiFT analysis yields the modulating low-frequency modes. Without Ca^{2+}, there is one prominent mode at ~175 cm^{-1}, the in-plane phenol ring rocking motion, likely providing directivity for the wavepacket moving out of the FC region toward ESPT barrier crossing. Upon Ca^{2+} binding, there are multiple competing modes below 300 cm^{-1} that result in an irregular oscillatory pattern in the first 2 ps. The fact that the 715 cm^{-1} mode shows clear oscillations while the 460 and 504 cm^{-1} modes do not, suggests a complex anharmonic coupling matrix between various vibrational normal modes[42,61,87,113,141,142] to project differently onto the multidimensional reaction coordinate of ESPT in the dynamic protein environment.

Notably, the second decay time constant that corresponds to ESPT in the Ca^{2+}-free GEM-GECO1 (~50 ps) is much longer than its counterpart in wtGFP (~5 ps). There seems to be some discrepancy with the aforementioned coherent proton movement that is prominent within 200 fs upon photoexcitation in the Ca^{2+}-free GEM-GECO1, but it is actually an indication of the multi-staged structural evolution that accompanies ESPT in these

constrained protein environments. The initial proton movement that induces the observed frequency blueshift of the 460 and 504 cm^{-1} modes is made possible by the pre-existing H-bonding chain that connects the phenolic hydroxyl group and the nearby in-plane serine residue (Ser118 in GEM-GECO1) via an intervening H_2O molecule.[61] However, a significant portion of proton transfer can only occur on a much longer timescale when the nearby protein residues including Ser118 and Glu135 as well as bridging H_2O molecules are geometrically optimized along the dynamic ESPT chain. In other words, the proton needs to be transferred farther away from the phenolic end toward the imidazolinone end of the chromophore to overcome the ESPT barrier. The significantly decreased ESPT rate in the Ca^{2+}-free GEM-GECO1 (vs. wtGFP) can thus be mainly attributed to labile H_2O molecules in the protein pocket because of its large β-barrel opening, even though the chromophore initially adopts a mostly in-plane phenolic ring rocking motion to facilitate ESPT.

V. Conclusion

In this contribution, we have used time-resolved FSRS to elucidate the multidimensional reaction coordinate for ESPT in a dual-emission Ca^{2+}-biosensor GEM-GECO1. Deeper structural dynamics insights are provided by the kinetic analysis of spectral signatures of several excited-state vibrational marker bands below 800 cm^{-1}. In difference from the previously reported modes above 1000 cm^{-1}, these lower frequency modes represent collective skeletal and HOOP motions that may be more sensitive to electronic redistribution over the chromophore ring system induced by *initial* coherent proton motions. The frequency blueshift of both 460 and 504 cm^{-1} modes within ~200 fs upon photoexcitation strongly

argues that some small-scale proton movement induces charge transfer from the phenolic hydroxyl end and the Ser223 hydroxyl end toward the chromophore ring system, effectively moving the photoexcited wavepackets from an LE to CT state on the excited-state PES. This represents a portion of the reaction coordinate that is largely insensitive to the protein environment. Once there, coherent low-frequency mode such as the ~175 cm^{-1} phenol ring rocking motion facilitates the optimization of the ESPT chain involving protein residues (Ser118, Glu135) and labile H_2O molecules in the Ca^{2+}-free protein, which overcomes the main ESPT reaction barrier and reaches the deprotonated fluorescent state to emit green.

For the Ca^{2+}-bound GEM-GECO1 with an altered protein pocket, the embedded chromophore adopts a more twisted conformation in S_0, which does not twist further in S_1. The frequency blueshift of the 460 and 504 cm^{-1} modes with faster time constant and smaller magnitude reveals that upon Ca^{2+} binding at the CaM domain, the GFP chromophore responds by implementing similar initial proton motions on a smaller scale following photoexcitation. Several coherent low-frequency modes below 300 cm^{-1} are retrieved from the intensity quantum beats of the 715 cm^{-1} mode, which suggest that anharmonically coupled "soft" low-frequency modes are collectively required to dissipate photoexcitation energy in lieu of ESPT. The fluorescence modulation mechanism in the GEM-GECO1 biosensor for Ca^{2+} imaging thus provides a paradigm to investigate the intricate relationship between a photoacidic chromophore and a Ca^{2+}-dependent protein environment, opening the door to mechanistically understand the structural dynamics basis and to rationally design the next-generation FP-based biosensors for metal-ion imaging in living systems.

Table 1. Kinetic data and vibrational mode assignment for three excited-state modes of GEM-GECO1 biosensor

S_1 FSRS[a] (cm^{-1})	S_1 Calc.[b] (cm^{-1})	S_0 FSRS (cm^{-1})	Kinetics[c] $-Ca^{2+}$	Kinetics[c] $+Ca^{2+}$	Vibrational mode assignment (major)[d]
455[e] 465[f]	487	448 450	(–) 1.3 ps (48%); 45 ps (52%)	(–) 1.4 ps (41%); 410 ps (59%)	Phenol ring HOOP, phenolic hydroxyl rocking, phenol ring deformation
503 504	527	507 509	(–) 1.4 ps (60%); 50 ps (40%)	(–) 1.5 ps (46%); 430 ps (54%)	Phenol ring HOOP and bridge-HOOP, serine[g] sidechain O–H wagging
715	675	750	(–) 1.8 ps (52%); 120 ps (48%)	(–) 2.0 ps (39%); 670 ps (61%)	Strong imidazolinone ring in-plane deformation, bridge CH motion, and small phenol ring-H rocking

[a]The frequency is reported as an average value of the FSRS vibrational mode frequencies between –100 fs and 1 ps to account for the spectral oscillatory behavior in the early time.

[b]The excited-state (S_1) vibrational frequencies of a geometrically optimized neutral SYG chromophore are calculated with TD-DFT RB3LYP 6-31G+(d,p) *in vacuo*. The calculated frequencies are all multiplied by a typical scaling factor of 0.96.

[c]The modes listed are associated with A* state of the photoexcited protonated chromophore.

[d]The major components for the mode assignment are described in correlation with Figure S5 in the Supporting Information. The largely coplanar two-ring system of the chromophore in the energy minimized, geometrically optimized structure is used to define the molecular plane. Therefore, the rocking/wagging represents the in-plane/out-of-plane (angular) bending motion, respectively. Due to the collective nature of these lower frequency vibrational

motions, we focus on the concentration of the modes on different parts of the chromophore as well as the involvement of phenolic hydroxyl, serine hydroxyl, and bridge CH atomic displacements in our interpretation of the time-resolved excited-state FSRS data.

[e]The stimulated Raman mode frequency in the Ca^{2+}-free GEM-GECO1 protein biosensor.

[f]The stimulated Raman mode frequency in the Ca^{2+}-bound GEM-GECO1 protein biosensor.

[g]This serine residue is part of the SYG chromophore (at the imidazolinone ring end) of GEM-GECO1.

Supporting Information Available: Figures S1-S8 showing unnormalized UV/Vis spectra, time-resolved FSRS data in S_1 with spectral baselines drawn, atomic displacements involved in three characteristic low-frequency modes, and kinetic plots of the excited-state FSRS marker band intensities of the Ca^{2+}-free and bound GEM-GECO1 biosensor. Discrete Fourier-transform analysis of the mode intensity oscillations in the 715 and 1265 cm^{-1} Raman modes. Tables S1-S2 displaying computed vibrational normal mode frequencies in both S_0 and S_1 of the SYG chromophore upon ring twisting and/or deprotonation. This material is available free of charge via the Internet at http://pubs.acs.org.

Acknowledgments. This work was supported by the Oregon State University Faculty Research Startup Grant and General Research Fund Award (to C.F.), Natural Sciences and Engineering Research Council of Canada & Canadian Institutes of Health Research (to R.E.C.), and a University of Alberta fellowship & an Alberta Innovates scholarship (to Y.Z.). R.E.C. holds a Tier II Canada Research Chair.

References:

(1) Shimomura, O.; Johnson, F. H.; Saiga, Y. Extraction, Purification and Properties of Aequorin, a Bioluminescent Protein from the Luminous Hydromedusan, *Aequorea*. *J. Cell. Comp. Physiol.* **1962**, *59*, 223-239.

(2) Matz, M. V.; Fradkov, A. F.; Labas, Y. A.; Savitsky, A. P.; Zaraisky, A. G.; Markelov, M. L.; Lukyanov, S. A. Fluorescent Proteins from Nonbioluminescent Anthozoa Species. *Nat. Biotechnol.* **1999**, *17*, 969-973.

(3) Vogt, A.; D'Angelo, C.; Oswald, F.; Denzel, A.; Mazel, C. H.; Matz, M. V.; Ivanchenko, S.; Nienhaus, G. U.; Wiedenmann, J. A Green Fluorescent Protein with Photoswitchable Emission from the Deep Sea. *PLoS ONE* **2008**, *3*, e3766.

(4) Shimomura, O. Structure of the Chromophore of *Aequorea* Green Fluorescent Protein. *FEBS Lett.* **1979**, *104*, 220-222.

(5) Chalfie, M.; Tu, Y.; Euskirchen, G.; Ward, W. W.; Prasher, D. C. Green Fluorescent Protein as a Marker for Gene Expression. *Science* **1994**, *263*, 802-805.

(6) Tsien, R. Y. The Green Fluorescent Protein. *Annu. Rev. Biochem.* **1998**, *67*, 509-544.

(7) Jung, G., (Ed.) *Fluorescent Proteins II: Application of Fluorescent Protein Technology*; Springer-Verlag: Berlin Heidelberg, 2012; Vol. 12.

(8) Campbell, R. E. Fluorescent Proteins. *Scholarpedia* **2008**, *3*, 5410.

(9) Betzig, E.; Patterson, G. H.; Sougrat, R.; Lindwasser, O. W.; Olenych, S.; Bonifacino, J. S.; Davidson, M. W.; Lippincott-Schwartz, J.; Hess, H. F. Imaging Intracellular Fluorescent Proteins at Nanometer Resolution. *Science* **2006**, *313*, 1642-1645.

(10) Rust, M. J.; Bates, M.; Zhuang, X. Sub-Diffraction-Limit Imaging by Stochastic Optical Reconstruction Microscopy (STORM). *Nat. Methods* **2006**, *3*, 793-796.

(11) Willig, K. I.; Kellner, R. R.; Medda, R.; Hein, B.; Jakobs, S.; Hell, S. W. Nanoscale Resolution in GFP-Based Microscopy. *Nat. Methods* **2006**, *3*, 721-723.

(12) Ai, H.-w.; Hazelwood, K. L.; Davidson, M. W.; Campbell, R. E. Fluorescent Protein FRET Pairs for Ratiometric Imaging of Dual Biosensors. *Nat. Methods* **2008**, *5*, 401-403.

(13) Andresen, M.; Stiel, A. C.; Folling, J.; Wenzel, D.; Schonle, A.; Egner, A.; Eggeling, C.; Hell, S. W.; Jakobs, S. Photoswitchable Fluorescent Proteins Enable Monochromatic Multilabel Imaging and Dual Color Fluorescence Nanoscopy. *Nat. Biotechnol.* **2008**, *26*, 1035-1040.

(14) Shcherbo, D.; Murphy, C. S.; Ermakova, G. V.; Solovieva, E. A.; Chepurnykh, T. V.; Shcheglov, A. S.; Verkhusha, V. V.; Pletnev, V. Z.; Hazelwood, K. L.; Roche, P. M.; et al. Far-Red Fluorescent Tags for Protein Imaging in Living Tissues. *Biochem. J.* **2009**, *418*, 567-574.

(15) Subach, F. V.; Patterson, G. H.; Manley, S.; Gillette, J. M.; Lippincott-Schwartz, J.; Verkhusha, V. V. Photoactivatable mCherry for High-Resolution Two-Color Fluorescence Microscopy. *Nat. Methods* **2009**, *6*, 153-159.

(16) Chudakov, D. M.; Matz, M. V.; Lukyanov, S.; Lukyanov, K. A. Fluorescent Proteins and Their Applications in Imaging Living Cells and Tissues. *Physiol. Rev.* **2010**, *90*, 1103-1163.

(17) Huang, B.; Babcock, H.; Zhuang, X. Breaking the Diffraction Barrier:

Super-Resolution Imaging of Cells. *Cell* **2010**, *143*, 1047-1058.

(18) Moeyaert, B.; Nguyen Bich, N.; De Zitter, E.; Rocha, S.; Clays, K.; Mizuno, H.; van Meervelt, L.; Hofkens, J.; Dedecker, P. Green-to-Red Photoconvertible Dronpa Mutant for Multimodal Super-resolution Fluorescence Microscopy. *ACS Nano* **2014**, *8*, 1664-1673.

(19) Stiel, A. C.; Andresen, M.; Bock, H.; Hilbert, M.; Schilde, J.; Schonle, A.; Eggeling, C.; Egner, A.; Hell, S. W.; Jakobs, S. Generation of Monomeric Reversibly Switchable Red Fluorescent Proteins for Far-Field Fluorescence Nanoscopy. *Biophys. J.* **2008**, *95*, 2989-2997.

(20) Moerner, W. E. New Directions in Single-Molecule Imaging and Analysis. *Proc. Natl. Acad. Sci. U.S.A.* **2007**, *104*, 12596-12602.

(21) Shaner, N. C.; Patterson, G. H.; Davidson, M. W. Advances in Fluorescent Protein Technology. *J. Cell Sci.* **2007**, *120*, 4247-4260.

(22) Jung, G., (Ed.) *Fluorescent Proteins I: From Understanding to Design*; Springer-Verlag: Berlin Heidelberg, 2012; Vol. 11.

(23) Kurplus, M.; McCammon, J. A. Dynamics of Proteins: Elements and Function. *Annu. Rev. Biochem.* **1983**, *52*, 263-300.

(24) Henzler-Wildman, K.; Kern, D. Dynamic Personalities of Proteins. *Nature* **2007**, *450*, 964-972.

(25) Akerboom, J.; Carreras Calderon, N.; Tian, L.; Wabnig, S.; Prigge, M.; Tolo, J.; Gordus, A.; Orger, M. B.; Severi, K. E.; Macklin, J. J.; et al. Genetically Encoded Calcium Indicators for Multi-Color Neural Activity Imaging and Combination with Optogenetics. *Front. Mol. Neurosci.* **2013**, *6*, 2.

(26) Chen, T.-W.; Wardill, T. J.; Sun, Y.; Pulver, S. R.; Renninger, S. L.; Baohan, A.; Schreiter, E. R.; Kerr, R. A.; Orger, M. B.; Jayaraman, V.; et al. Ultrasensitive Fluorescent Proteins for Imaging Neuronal Activity. *Nature* **2013**, *499*, 295-300.

(27) Davidson, M. W.; Campbell, R. E. Engineered Fluorescent Proteins: Innovations and Applications. *Nat. Methods* **2009**, *6*, 713-717.

(28) Zhao, Y.; Araki, S.; Wu, J.; Teramoto, T.; Chang, Y.-F.; Nakano, M.; Abdelfattah, A. S.; Fujiwara, M.; Ishihara, T.; Nagai, T.; et al. An Expanded Palette of Genetically Encoded Ca^{2+} Indicators. *Science* **2011**, *333*, 1888-1891.

(29) Tian, L.; Hires, S. A.; Mao, T.; Huber, D.; Chiappe, M. E.; Chalasani, S. H.; Petreanu, L.; Akerboom, J.; McKinney, S. A.; Schreiter, E. R.; et al. Imaging Neural Activity in Worms, Flies and Mice with Improved GCaMP Calcium Indicators. *Nat. Methods* **2009**, *6*, 875-881.

(30) Akerboom, J.; Chen, T.-W.; Wardill, T. J.; Tian, L.; Marvin, J. S.; Mutlu, S.; Calderón, N. C.; Esposti, F.; Borghuis, B. G.; Sun, X. R.; et al. Optimization of a GCaMP Calcium Indicator for Neural Activity Imaging. *J. Neurosci.* **2012**, *32*, 13819-13840.

(31) Walker, A. S.; Burrone, J.; Meyer, M. P. Functional Imaging in the Zebrafish Retinotectal System using RGECO. *Front. Neural Circuits* **2013**, *7*, 34.

(32) Lecrone, V.; Li, W.; Devoll, R. E.; Logothetis, C.; Farach-Carson, M. C. Calcium Signals in Prostate Cancer Cells: Specific Activation by Bone-Matrix Proteins. *Cell Calcium* **2000**, *27*, 35-42.

(33) Prevarskaya, N.; Skryma, R.; Shuba, Y. Calcium in Tumour Metastasis: New Roles for Known Actors. *Nat. Rev. Cancer* **2011**, *11*, 609-618.

(34) Nagai, T.; Sawano, A.; Park, E. S.; Miyawaki, A. Circularly Permuted Green Fluorescent Proteins Engineered to Sense Ca^{2+}. *Proc. Natl. Acad. Sci. U.S.A.* **2001**, *98*, 3197-3202.

(35) Nakai, J.; Ohkura, M.; Imoto, K. A High Signal-to-noise Ca^{2+} Probe Composed of a Single Green Fluorescent Protein. *Nat. Biotechnol.* **2001**, *19*, 137-141.

(36) Wang, Q.; Shui, B.; Kotlikoff, M. I.; Sondermann, H. Structural Basis for Calcium Sensing by GCaMP2. *Structure* **2008**, *16*, 1817-1827.

(37) Akerboom, J.; Rivera, J. D. V.; Guilbe, M. M. R.; Malavé, E. C. A.; Hernandez, H. H.; Tian, L.; Hires, S. A.; Marvin, J. S.; Looger, L. L.; Schreiter, E. R. Crystal Structures of the GCaMP Calcium Sensor Reveal the Mechanism of Fluorescence Signal Change and Aid Rational Design. *J. Biol. Chem.* **2009**, *284*, 6455-6464.

(38) Barnett, M. W.; Larkman, P. M. The Action Potential. *Pract. Neurol.* **2007**, *7*, 192-197.

(39) Chattoraj, M.; King, B. A.; Bublitz, G. U.; Boxer, S. G. Ultra-Fast Excited State Dynamics in Green Fluorescent Protein: Multiple States and Proton Transfer. *Proc. Natl. Acad. Sci. U.S.A.* **1996**, *93*, 8362-8367.

(40) Ormo, M.; Cubitt, A. B.; Kallio, K.; Gross, L. A.; Tsien, R. Y.; Remington, S. J. Crystal Structure of the *Aequorea victoria* Green Fluorescent Protein. *Science* **1996**, *273*, 1392-1395.

(41) Yang, F.; Moss, L. G.; Phillips, G. N., Jr. The Molecular Structure of Green Fluorescent Protein. *Nat. Biotechnol.* **1996**, *14*, 1246-1251.

(42) Fang, C.; Frontiera, R. R.; Tran, R.; Mathies, R. A. Mapping GFP Structure

Evolution during Proton Transfer with Femtosecond Raman Spectroscopy. *Nature* **2009**, *462*, 200-204.

(43) Mukamel, S.; Biggs, J. D. Communication: Comment on the Effective Temporal and Spectral Resolution of Impulsive Stimulated Raman Signals. *J. Chem. Phys.* **2011**, *134*, 161101.

(44) Frontiera, R. R.; Fang, C.; Dasgupta, J.; Mathies, R. A. Probing Structural Evolution along Multidimensional Reaction Coordinates with Femtosecond Stimulated Raman Spectroscopy. *Phys. Chem. Chem. Phys.* **2012**, *14*, 405-414.

(45) Lossau, H.; Kummer, A.; Heinecke, R.; Pollinger-Dammer, F.; Kompa, C.; Bieser, G.; Jonsson, T.; Silva, C. M.; Yang, M. M.; Youvan, D. C.; et al. Time-Resolved Spectroscopy of Wild-Type and Mutant Green Fluorescent Proteins Reveals Excited State Deprotonation Consistent with Fluorophore-Protein Interactions. *Chem. Phys.* **1996**, *213*, 1-16.

(46) Jung, G.; Wiehler, J.; Zumbusch, A. The Photophysics of Green Fluorescent Protein: Influence of the Key Amino Acids at Positions 65, 203, and 222. *Biophys. J.* **2005**, *88*, 1932-1947.

(47) Jaye, A. A.; Stoner-Ma, D.; Matousek, P.; Towrie, M.; Tonge, P. J.; Meech, S. R. Time-Resolved Emission Spectra of Green Fluorescent Protein. *Photochem. Photobiol.* **2006**, *82*, 373-379.

(48) Cinelli, R. A. G.; Tozzini, V.; Pellegrini, V.; Beltram, F.; Cerullo, G.; Zavelani-Rossi, M.; De Silvestri, S.; Tyagi, M.; Giacca, M. Coherent Dynamics of Photoexcited Green Fluorescent Proteins. *Phys. Rev. Lett.* **2001**, *86*, 3439-3442.

(49) Kennis, J. T. M.; Larsen, D. S.; Stokkum, I. H. M. v.; Vengris, M.; Thor, J. J. v.; Grondelle, R. v. Uncovering the Hidden Ground State of Green Fluorescent Protein. *Proc. Natl. Acad. Sci. USA* **2004**, *101*, 17988-17993.

(50) Stoner-Ma, D.; Jaye, A. A.; Matousek, P.; Towrie, M.; Meech, S. R.; Tonge, P. J. Observation of Excited-State Proton Transfer in Green Fluorescent Proetin using Ultrafast Vibrational Spectroscopy. *J. Am. Chem. Soc.* **2005**, *127*, 2864-2865.

(51) Stoner-Ma, D.; Melief, E. H.; Nappa, J.; Ronayne, K. L.; Tonge, P. J.; Meech, S. R. Proton Relay Reaction in Green Fluorescent Protein (GFP): Polarization-Resolved Ultrafast Vibrational Spectroscopy of Isotopically Edited GFP. *J. Phys. Chem. B* **2006**, *110*, 22009-22018.

(52) Stoner-Ma, D.; Jaye, A. A.; Ronayne, K. L.; Nappa, J.; Tonge, P. J.; Meech, S. R. Ultrafast Electronic and Vibrational Dynamics of Stabilized A State Mutants of the Green Fluorescent Protein (GFP): Snipping the Proton Wire. *Chem. Phys.* **2008**, *350*, 193-200.

(53) Meech, S. R. Excited State Reactions in Fluorescent Proteins. *Chem. Soc. Rev.* **2009**, *38*, 2922-2934.

(54) van Thor, J. J.; Zanetti, G.; Ronayne, K. L.; Towrie, M. Structural Events in the Photocycle of Green Fluorescent Protein. *J. Phys. Chem. B* **2005**, *109*, 16099-16108.

(55) McHale, J. L. *Molecular Spectroscopy*; Prentice-Hall: Upper Saddle River, NJ, 1999.

(56) Chudoba, C.; Riedle, E.; Pfeiffer, M.; Elsaesser, T. Vibrational Coherence in Ultrafast Excited State Proton Transfer. *Chem. Phys. Lett.* **1996**, *263*, 622-628.

(57) Heyne, K.; Huse, N.; Dreyer, J.; Nibbering, E. T. J.; Elsaesser, T.; Mukamel, S.

Coherent Low-Frequency Motions of Hydrogen Bonded Acetic Acid Dimers in the Liquid Phase. *J. Chem. Phys.* **2004**, *121*, 902-913.

(58) Yamada, Y.; Mikoshiba, K. Quantitative Comparison of Novel GCaMP-type Genetically Encoded Ca^{2+} Indicators in Mammalian Neurons. *Front. Cell. Neurosci.* **2012**, *6*, 41.

(59) Chen, Y.; Song, X.; Ye, S.; Miao, L.; Zhu, Y.; Zhang, R.-G.; Ji, G. Structural Insight into Enhanced Calcium Indicator GCaMP3 and GCaMPJ to Promote Further Improvement. *Protein Cell* **2013**, *4*, 299-309.

(60) Frisch, M. J.; Trucks, G. W.; Schlegel, H. B.; Scuseria, G. E.; Robb, M. A.; Cheeseman, J. R.; Scalmani, G.; Barone, V.; Mennucci, B.; Petersson, G. A.; et al. Gaussian 09, Revision B.1; Gaussian, Inc.: Wallingford, CT, 2009.

(61) Oscar, B. G.; Liu, W.; Zhao, Y.; Tang, L.; Wang, Y.; Campbell, R. E.; Fang, C. Excited-State Structural Dynamics of a Dual-Emission Calmodulin-Green Fluorescent Protein Sensor for Calcium Ion Imaging. *Proc. Natl. Acad. Sci. U.S.A.* **2014**, *111*, 10191-10196.

(62) Liu, W.; Han, F.; Smith, C.; Fang, C. Ultrafast Conformational Dynamics of Pyranine during Excited State Proton Transfer in Aqueous Solution Revealed by Femtosecond Stimulated Raman Spectroscopy. *J. Phys. Chem. B* **2012**, *116*, 10535-10550.

(63) Han, F.; Liu, W.; Fang, C. Excited-State Proton Transfer of Photoexcited Pyranine in Water Observed by Femtosecond Stimulated Raman Spectroscopy. *Chem. Phys.* **2013**, *422*, 204-219.

(64) Wang, Y.; Liu, W.; Tang, L.; Oscar, B. G.; Han, F.; Fang, C. Early Time

Excited-State Structural Evolution of Pyranine in Methanol Revealed by Femtosecond Stimulated Raman Spectroscopy. *J. Phys. Chem. A* **2013**, *117*, 6024-6042.

(65) Brejc, K.; Sixma, T. K.; Kitts, P. A.; Kain, S. R.; Tsien, R. Y.; Ormö, M.; Remington, S. J. Structural Basis for Dual Excitation and Photoisomerization of the *Aequorea victoria* Green Fluorescent Protein. *Proc. Natl. Acad. Sci. U.S.A.* **1997**, *94*, 2306-2311.

(66) Humphrey, W.; Dalke, A.; Schulten, K. VMD - Visual Molecular Dynamics. *J. Mol. Graphics* **1996**, *14*, 33-38.

(67) Hanson, G. T.; McAnaney, T. B.; Park, E. S.; Rendell, M. E. P.; Yarbrough, D. K.; Chu, S.; Xi, L.; Boxer, S. G.; Montrose, M. H.; Remington, S. J. Green Fluorescent Protein Variants as Ratiometric Dual Emission pH Sensors. 1. Structural Characterization and Preliminary Application. *Biochemistry* **2002**, *41*, 15477-15488.

(68) Drobizhev, M.; Makarov, N. S.; Tillo, S. E.; Hughes, T. E.; Rebane, A. Two-Photon Absorption Properties of Fluorescent Proteins. *Nat. Meth.* **2011**, *8*, 393-399.

(69) Bell, A. F.; He, X.; Wachter, R. M.; Tonge, P. J. Probing the Ground State Structure of the Green Fluorescent Protein Chromophore using Raman Spectroscopy. *Biochemistry* **2000**, *39*, 4423-4431.

(70) Schellenberg, P.; Johnson, E.; Esposito, A. P.; Reid, P. J.; Parson, W. W. Resonance Raman scattering by the green fluorescent protein and an analogue of its chromophore. *J. Phys. Chem. B* **2001**, *105*, 5316-5322.

(71) He, X.; Bell, A. F.; Tonge, P. J. Isotopic labeling and normal-mode analysis of a model green fluorescent protein chromophore. *J. Phys. Chem. B* **2002**, *106*, 6056-6066.

(72) Tozzini, V.; Nifosì, R. Ab Initio Molecular Dynamics of the Green Fluorescent Protein (GFP) Chromophore: An Insight into the Photoinduced Dynamics of Green Fluorescent Proteins. *J. Phys. Chem. B* **2001**, *105*, 5797-5803.

(73) Tozzini, V.; Bizzarri, A. R.; Pellegrini, V.; Nifosi, R.; Giannozzi, P.; Iuliano, A.; Cannistraro, S.; Beltram, F. The Low Frequency Vibrational Modes of Green Fluorescent Proteins. *Chem. Phys.* **2003**, *287*, 33-42.

(74) Gnanasekaran, R. Normal Modes and the Duschinsky Mixing of the Ground- and Excited-State Vibrations of the Green Fluorescent Protein Chromophore. *Chem. Phys. Lett.* **2013**, *587*, 61-67.

(75) Savarese, M.; Netti, P. A.; Adamo, C.; Rega, N.; Ciofini, I. Exploring the Metric of Excited State Proton Transfer Reactions. *J. Phys. Chem. B* **2013**, *117*, 16165-16173.

(76) Gozem, S.; Melaccio, F.; Luk, H. L.; Rinaldi, S.; Olivucci, M. Learning from Photobiology How to Design Molecular Devices using a Computer. *Chem. Soc. Rev.* **2014**, *43*, 4019-4036.

(77) Follenius-Wund, A.; Bourotte, M.; Schmitt, M.; Iyice, F.; Lami, H.; Bourguignon, J.-J.; Haiech, J.; Pigault, C. Fluorescent Derivatives of the GFP Chromophore Give a New Insight into the GFP Fluorescence Process. *Biophys. J.* **2003**, *85*, 1839-1850.

(78) Vengris, M.; van Stokkum, I. H. M.; He, X.; Bell, A. F.; Tonge, P. J.; van Grondelle, R.; Larsen, D. S. Ultrafast Excited and Ground-State Dynamics of the Green Fluorescent Protein Chromophore in Solution. *J. Phys. Chem. A* **2004**, *108*, 4587-4598.

(79) Kukura, P.; McCamant, D. W.; Yoon, S.; Wandschneider, D. B.; Mathies, R. A. Structural Observation of the Primary Isomerization in Vision with Femtosecond-Stimulated

Raman. *Science* **2005**, *310*, 1006-1009.

(80) Chen, M. C.; Lambert, C. R.; Urgitis, J. D.; Zimmer, M. Photoisomerization of Green Fluorescent Protein and the Dimensions of the Chromophore Cavity. *Chem. Phys.* **2001**, *270*, 157-164.

(81) Rafiq, S.; Rajbongshi, B. K.; Nair, N. N.; Sen, P.; Ramanathan, G. Excited State Relaxation Dynamics of Model Green Fluorescent Protein Chromophore Analogs: Evidence for Cis-Trans Isomerism. *J. Phys. Chem. A* **2011**, *115*, 13733-13742.

(82) Baffour-Awuah, N. Y. A.; Zimmer, M. Hula-Twisting in Green Fluorescent Protein. *Chem. Phys.* **2004**, *303*, 7-11.

(83) Maddalo, S. L.; Zimmer, M. The Role of the Protein Matrix in Green Fluorescent Protein Fluorescence. *Photochem. Photobiol.* **2006**, *82*, 367-372.

(84) McCamant, D. W.; Kukura, P.; Yoon, S.; Mathies, R. A. Femtosecond Broadband Stimulated Raman Spectroscopy: Apparatus and Methods. *Rev. Sci. Instrum.* **2004**, *75*, 4971-4980.

(85) Kukura, P.; McCamant, D. W.; Mathies, R. A. Femtosecond Stimulated Raman Spectroscopy. *Annu. Rev. Phys. Chem.* **2007**, *58*, 461-488.

(86) Zhu, L.; Liu, W.; Fang, C. Tunable Sideband Laser from Cascaded Four-Wave Mixing in Thin Glass for Ultra-Broadband Femtosecond Stimulated Raman Spectroscopy. *Appl. Phys. Lett.* **2013**, *103*, 061110.

(87) Levine, B. G.; Martínez, T. J. Isomerization Through Conical Intersections. *Annu. Rev. Phys. Chem.* **2007**, *58*, 613-634.

(88) Takeuchi, S.; Ruhman, S.; Tsuneda, T.; Chiba, M.; Taketsugu, T.; Tahara, T.

Spectroscopic Tracking of Structural Evolution in Ultrafast Stilbene Photoisomerization. *Science* **2008**, *322*, 1073-1077.

(89) Weber, W.; Helms, V.; McCammon, J. A.; Langhoff, P. W. Shedding Light on the Dark and Weakly Fluorescent States of Green Fluorescent Proteins. *Proc. Natl. Acad. Sci. U.S.A.* **1999**, *96*, 6177-6182.

(90) Shinobu, A.; Palm, G. J.; Schierbeek, A. J.; Agmon, N. Visualizing Proton Antenna in a High-Resolution Green Fluorescent Protein Structure. *J. Am. Chem. Soc.* **2010**, *132*, 11093-11102.

(91) Granucci, G.; Hynes, J. T.; Millie, P.; Tran-Thi, T.-H. A Theoretical Investigation of Excited-State Acidity of Phenol and Cyanophenols. *J. Am. Chem. Soc.* **2000**, *122*, 12243-12253.

(92) Hynes, J. T.; Tran-Thi, T.-H.; Granucci, G. Intermolecular Photochemical Proton Transfer in Solution: New Insights and Perspectives. *J. Photochem. Photobiol. A Chem.* **2002**, *154*, 3-11.

(93) Fang, C.; Senes, A.; Cristian, L.; DeGrado, W. F.; Hochstrasser, R. M. Amide Vibrations Are Delocalized Across the Hydrophobic Interface of a Transmembrane Helix Dimer. *Proc. Natl. Acad. Sci. USA* **2006**, *103*, 16740-16745.

(94) Hochstrasser, R. M. Two-Dimensional Spectroscopy at Infrared and Optical Frequencies. *Proc. Natl. Acad. Sci. USA* **2007**, *104*, 14190-14196.

(95) Woys, A. M.; Almeida, A. M.; Wang, L.; Chiu, C.-C.; McGovern, M.; de Pablo, J. J.; Skinner, J. L.; Gellman, S. H.; Zanni, M. T. Parallel β-Sheet Vibrational Couplings Revealed by 2D IR Spectroscopy of an Isotopically Labeled Macrocycle: Quantitative

Benchmark for the Interpretation of Amyloid and Protein Infrared Spectra. *J. Am. Chem. Soc.* **2012**, *134*, 19118-19128.

(96) Cina, J. A.; Kovac, P. A. How Fissors Works: Observing Vibrationally Adiabatic Conformational Change through Femtosecond Stimulated Raman Spectroscopy. *J. Phys. Chem. A* **2013**, *117*, 6084-6095.

(97) Zheltikov, A. Editorial: Supercontinuum Generation. *Appl. Phys. B* **2003**, *77*, 143-147.

(98) Liu, W.; Zhu, L.; Wang, L.; Fang, C. Cascaded Four-Wave Mixing for Broadband Tunable Laser Sideband Generation. *Opt. Lett.* **2013**, *38*, 1772-1774.

(99) Fang, C.; Hochstrasser, R. M. Two-Dimensional Infrared Spectra of the $^{13}C=^{18}O$ Isotopomers of Alanine Residues in an α-Helix. *J. Phys. Chem. B* **2005**, *109*, 18652-18663.

(100) Di Donato, M.; van Wilderen, L. J. G. W.; Van Stokkum, I. H. M.; Stuart, T. C.; Kennis, J. T. M.; Hellingwerf, K. J.; van Grondelle, R.; Groot, M. L. Proton Transfer Events in GFP. *Phys. Chem. Chem. Phys.* **2011**, *13*, 16295-16305.

(101) Felker, P. M.; Zewail, A. H. Dynamics of Intramolecular Vibrational-Energy Redistribution (IVR). I. Coherence Effects. *J. Chem. Phys.* **1985**, *82*, 2961-2974.

(102) Owrutsky, J. C.; Raftery, D.; Hochstrasser, R. M. Vibrational Relaxation Dynamics in Solutions. *Annu. Rev. Phys. Chem.* **1994**, *45*, 519-555.

(103) Hamm, P.; Lim, M.; Hochstrasser, R. M. Structure of the Amide I Band of Peptides Measured by Femtosecond Nonlinear-Infrared Spectroscopy. *J. Phys. Chem. B* **1998**, *102*, 6123-6138.

(104) Myers, A. B.; Mathies, R. A. Resonance Raman intensities: A Probe of

Excited-State Structure and Dynamics. In *Biological Applications of Raman Spectroscopy*; Spiro, T. G., Ed.; John Wiley & Sons, Inc.: New York, 1987; Vol. 2; pp 1-58.

(105) Nibbering, E. T. J.; Fidder, H.; Pines, E. Ultrafast Chemistry: Using Time-Resolved Vibrational Spectroscopy for Interrogation of Structural Dynamics. *Annu. Rev. Phys. Chem.* **2005**, *56*, 337-367.

(106) Polli, D.; Altoè, P.; Weingart, O.; Spillane, K. M.; Manzoni, C.; Brida, D.; Tomasello, G.; Orlandi, G.; Kukura, P.; Mathies, R. A.; et al. Conical Intersection Dynamics of the Primary Photoisomerization Event in Vision. *Nature* **2010**, *467*, 440-443.

(107) Wörner, H. J.; Corkum, P. B. Attosecond Spectroscopy. In *Handbook of High-resolution Spectroscopy*; John Wiley & Sons, Ltd: Hoboken, NJ, 2011.

(108) Mohammed, O. F.; Dreyer, J.; magnes, B.-Z.; Pines, E.; Nibbering, E. T. J. Solvent-Dependent Photoacidity State of Pyranine Monitored by Transient Mid-Infrared Spectroscopy. *ChemPhysChem* **2005**, *6*, 625-636.

(109) Shi, X.; Abbyad, P.; Shu, X.; Kallio, K.; Kanchanawong, P.; Childs, W.; Remington, S. J.; Boxer, S. G. Ultrafast Excited-State Dynamics in the Green Fluorescent Protein Variant S65T/H148D. 2. Unusual Photophysical Properties. *Biochemistry* **2007**, *46*, 12014-12025.

(110) Kondo, M.; Heisler, I. A.; Stoner-Ma, D.; Tonge, P. J.; Meech, S. R. Ultrafast Dynamics of Protein Proton Transfer on Short Hydrogen Bond Potential Energy Surfaces: S65T/H148D GFP. *J. Am. Chem. Soc.* **2010**, *132*, 1452-1453.

(111) Tolbert, L. M.; Solntsev, K. M. Excited-State Proton Transfer: From Constrained Systems to "Super" Photoacids to Superfast Proton Transfer. *Acc. Chem. Res.*

2002, *35*, 19-27.

(112) Vos, M. H.; Rappaport, F.; Lambry, J.-C.; Breton, J.; Martin, J.-L. Visualization of Coherent Nuclear Motion in a Membrane Protein by Femtosecond Spectroscopy. *Nature* **1993**, *363*, 320-325.

(113) Wang, Q.; Schoenlein, R. W.; Peteanu, L. A.; Mathies, R. A.; Shank, C. V. Vibrationally Coherent Photochemistry in the Femtosecond Primary Event of Vision. *Science* **1994**, *266*, 422-424.

(114) Zhu, L.; Sage, J. T.; Champion, P. M. Observation of Coherent Reaction Dynamics in Heme Proteins. *Science* **1994**, *266*, 629-632.

(115) Kummer, A. D.; Wiehler, J.; Rehaber, H.; Kompa, C.; Steipe, B.; Michel-Beyerle, M. E. Effects of Threonine 203 Replacements on Excited-State Dynamics and Fluorescence Properties of the Green Fluorescent Protein (GFP). *J. Phys. Chem. B* **2000**, *104*, 4791-4798.

(116) Mandal, D.; Tahara, T.; Meech, S. R. Excited-State Dynamics in the Green Fluorescent Protein Chromophore. *J. Phys. Chem. B* **2004**, *108*, 1102-1108.

(117) Shu, X.; Leiderman, P.; Gepshtein, R.; Smith, N. R.; Kallio, K.; Huppert, D.; Remington, S. J. An Alternative Excited-State Proton Transfer Pathway in Green Fluorescent Protein Variant S205V. *Protein Sci.* **2007**, *16*, 2703-2710.

(118) Miyawaki, A.; Llopis, J.; Heim, R.; McCaffery, J. M.; Adams, J. A.; Ikura, M.; Tsien, R. Y. Fluorescent Indicators for Ca^{2+} Based on Green Fluorescent Proteins and Calmodulin. *Nature* **1997**, *388*, 882-887.

(119) Petrone, A.; Caruso, P.; Tenuta, S.; Rega, N. On the Optical Absorption of the

Anionic GFP Chromophore in Vacuum, Solution, and Protein. *Phys. Chem. Chem. Phys.* **2013**, *15*, 20536-20544.

(120) Ishikita, H.; Saito, K. Proton Transfer Reactions and Hydrogen-Bond Networks in Protein Environments. *J. R. Soc. Interface* **2014**, *11*, 20130518.

(121) Zimmer, M. Green Fluorescent Protein (GFP): Applications, Structure, and Related Photophysical Behavior. *Chem. Rev.* **2002**, *102*, 759-781.

(122) Kojima, S.; Ohkawa, H.; Hirano, T.; Maki, S.; Niwa, H.; Ohashi, M.; Inouye, S.; Tsuji, F. I. Fluorescent Properties of Model Chromophores of Tyrosine-66 Substituted Mutants of *Aequorea* Green Fluorescent Protein (GFP). *Tetra. Lett.* **1998**, *39*, 5239-5242.

(123) Baranov, M. S.; Lukyanov, K. A.; Borissova, A. O.; Shamir, J.; Kosenkov, D.; Slipchenko, L. V.; Tolbert, L. M.; Yampolsky, I. V.; Solntsev, K. M. Conformationally Locked Chromophores as Models of Excited-State Proton Transfer in Fluorescent Proteins. *J. Am. Chem. Soc.* **2012**, *134*, 6025-6032.

(124) Hynes, J. T. Physical Chemistry: The Protean Proton in Water. *Nature* **1999**, *397*, 565-567.

(125) Westlake, B. C.; Brennaman, M. K.; Concepcion, J. J.; Paul, J. J.; Bettis, S. E.; Hampton, S. D.; Miller, S. A.; Lebedeva, N. V.; Forbes, M. D. E.; Moran, A. M.; et al. Concerted Electron-Proton Transfer in the Optical Excitation of Hydrogen-Bonded Dyes. *Proc. Natl. Acad. Sci. U.S.A.* **2011**, *108*, 8554-8558.

(126) Petkova, I.; Dobrikov, G.; Banerji, N.; Duvanel, G.; Perez, R.; Dimitrov, V.; Nikolov, P.; Vauthey, E. Tuning the Excited-State Dynamics of GFP-Inspired Imidazolone Derivatives. *J. Phys. Chem. A* **2010**, *114*, 10-20.

(127) Hammes-Schiffer, S. When Electrons and Protons Get Excited. *Proc. Natl. Acad. Sci. U.S.A.* **2011**, *108*, 8531-8532.

(128) Solntsev, K. M.; Huppert, D.; Tolbert, L. M.; Agmon, N. Solvatochromic Shifts of "Super" Photoacids. *J. Am. Chem. Soc.* **1998**, *120*, 7981-7982.

(129) Agmon, N. Elementary Steps in Excited-State Proton Transfer. *J. Phys. Chem. A* **2005**, *109*, 13-35.

(130) Cox, M. J.; Timmer, R. L. A.; Bakker, H. J.; Park, S.; Agmon, N. Distance-Dependent Proton Transfer along Water Wires Connecting Acid-Base Pairs. *J. Phys. Chem. A* **2009**, *113*, 6599-6606.

(131) Kulig, W.; Agmon, N. A 'Clusters-in-Liquid' Method for Calculating Infrared Spectra Identifies the Proton-Transfer Mode in Acidic Aqueous Solutions. *Nat. Chem.* **2013**, *5*, 29-35.

(132) Siwick, B. J.; Bakker, H. J. On the Role of Water in Intermolecular Proton-Transfer Reactions. *J. Am. Chem. Soc.* **2007**, *129*, 13412-13420.

(133) Siwick, B. J.; Cox, M. J.; Bakker, H. J. Long-Range Proton Transfer in Aqueous Acid-Base Reactions. *J. Phys. Chem. B* **2008**, *112*, 378-389.

(134) Rini, M.; Magnes, B.-Z.; Pines, E.; Nibbering, E. T. J. Real-Time Observation of Bimodal Proton Transfer in Acid-Base Pairs in Water. *Science* **2003**, *301*, 349-352.

(135) Rini, M.; Pines, D.; Magnes, B. Z.; Pines, E.; Nibbering, E. T. J. Bimodal Proton Transfer in Acid-Base Reactions in Water. *J. Chem. Phys.* **2004**, *121*, 9593-9610.

(136) Mohammed, O. F.; Pines, D.; Dreyer, J.; Pines, E.; Nibbering, E. T. J. Sequential Proton Transfer through Water Bridges in Acid-Base Reactions. *Science* **2005**,

310, 83-86.

(137) Elsaesser, T.; Huse, N.; Dreyer, J.; Dwyer, J. R.; Heyne, K.; Nibbering, E. T. J. Ultrafast Vibrational Dynamics and Anharmonic Couplings of Hydrogen-Bonded Dimers in Solution. *Chem. Phys.* **2007**, *341*, 175-188.

(138) Premont-Schwarz, M.; Barak, T.; Pines, D.; Nibbering, E. T. J.; Pines, E. Ultrafast Excited-State Proton-Transfer Reaction of 1-Naphthol-3,6-Disulfonate and Several 5-Substituted 1-Naphthol Derivatives. *J. Phys. Chem. B* **2013**, *117*, 4594-4603.

(139) Tran-Thi, T.-H.; Gustavsson, T.; Prayer, C.; Pommeret, S.; Hynes, J. T. Primary Ultrafast Events Preceding the Photoinduced Proton Transfer from Pyranine to Water. *Chem. Phys. Lett.* **2000**, *329*, 421-430.

(140) Agmon, N. The Grotthuss Mechanism. *Chem. Phys. Lett.* **1995**, *244*, 456-462.

(141) Wilson, K. C.; Lyons, B.; Mehlenbacher, R.; Sabatini, R.; McCamant, D. W. Two-Dimensional Femtosecond Stimulated Raman Spectroscopy: Observation of Cascading Raman Signals in Acetonitrile. *J. Chem. Phys.* **2009**, *131*, 214502-214515.

(142) Hoffman, D. P.; Ellis, S. R.; Mathies, R. A. Characterization of a Conical Intersection in a Charge-Transfer Dimer with Two-Dimensional Time-Resolved Stimulated Raman Spectroscopy. *J. Phys. Chem. A* **2014**, *118*, 4955-4965.

Table of Contents (TOC) Image

(in the actual size to be used)